Christoph Nausner

Diffusional Kurtosis Imaging

Diploma

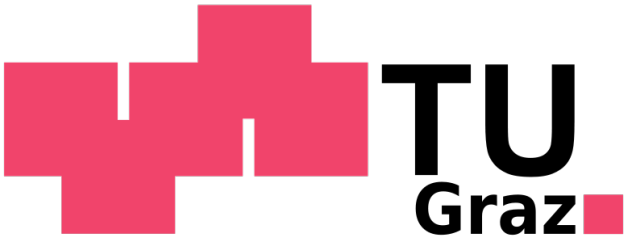

Institute of Medical Engineering
Graz University of Technology
Kronesgasse 5, A - 8010 Graz
Head: Univ.-Prof. Dipl.-Ing. Dr.techn. Rudolf Stollberger

Supervisor: Univ.-Prof. Dipl.-Ing. Dr.techn. Rudolf Stollberger

Graz, (April, 2012)

Zusammenfassung

In vivo Magnetresonanz (MR) kann zur nicht invasiven Erfassung der mikroskopischen Bewegung von Wasser im Körper verwendet werden. Die Selbstdiffusion von Wassermolekülen führt zu einem Signalintensitätsabnahme bei Verwendung von Diffusionsgradienten. Diese Gradienten werden in der MR zur Diffusionscodierung mit mehreren b-Faktoren verwendet. Die resultierende Signalintensitätsabnahme kann durch eine bi- oder multi-exponentielle Funktion beschrieben werden. Die Parameter dieses Fits sind sehr Rauschempfindlich und beschreiben nur dann tatsächlich physiologische Eigenschaften, wenn es sich um mehrere Diffusions-Pools mit gaußscher Diffusion handelt. Im Gegensatz dazu hat die Diffusions-Kurtosis-Bildgebung nicht diese Einschränkung und ein besseres Rauschverhalten. Es wird eine Taylorreihe zweiter Ordnung verwendet wodurch sie bei hoher Diffusionsgewichtung einen systematischen Fehler hat. Die Aufgabe dieser Arbeit war es zu versuchen die optimalen b-Faktoren für die Diffusions-Kurtosis-Bildgebung zu finden und die Parameter zu identifizieren. Aus diesem Grund wurde ein Computermodell zur Simulation von weißem Gewebe entwickelt, dass auf einer Monte Carlo Methode beruht. Durch dieses Modell konnte ein möglicher Zusammenhang zwischen der scheinbaren Diffusionskonstante und dem Gewebe unter Berücksichtigung der Daten des dazugehörigen $T2$-gewichteten Bildes gefunden werden.

Schlagwörter: Magnetresonanz; Diffusionsbildgebung; Diffusions-Kurtosis-Bildgebung; Monte Carlo Methode; Simulation der Wasserbewegung

Abstract

In vivo nuclear magnetic resonance (NMR) is used to acquire the microscopic movements of water in a non-invasive way. The self-diffusion of water seems to be restricted by the tissue. The measured signal intensity shows a multi-exponential decay. A fast and a slow diffusion pool were suggested to describe the signal. This fit only represents the physiological properties, if the water pools have Gaussian distributed diffusion. Since the parameters are noise sensitive errors due to misinterpretation are possible. The later introduced Diffusional-Kurtosis-Imaging (DKI) doesn't show the same restriction as the bi-exponential model and seems to be less noise sensitive. A Taylor series of second order is used in the exponent to fit the non-mono-exponential signal intensity decay. This causes a systematic error at high diffusion weightings. The aim the present work was to identify the fitted Parameters and compare the different models. For this reason a model of the white matter (WM), which is based on a Monte Carlo Method, was developed to simulate the movement of water and estimate the optimal diffusion weights and identify the parameters. If the apparent diffusion coefficient (ADC) is linked to a $T2$-weighted image it seems to reveal knowledge of the underlying tissue. The apparent kurtosis coefficient (AKC) appears to be only useful as an estimation of the error in with our current knowledge.

Keywords: nuclear magnetic resonance; diffusion weighted imaging; diffusional kurtosis imaging; Monte Carlo method; simulation of water movement

Contents

List of Figures

List of Tables

1 Introduction

1.1 Topic of the Present Work

Most of the Human brain (70% of the volume, 90% of the mass) is water [9]. Therefore the behaviour of water plays an important role in the human physiology and may be an indicator for tissue properties. Diffusion weighted magnetic resonance imaging (DW-MRI) is an imaging method to estimate the water movement within cells, the extracellular space and the exchange between these water pools. It is already used to detect possible pathological changes in the human brain (for example in case of ischemic cerebral vasculitis, diffusion changes significantly compared to physiological behaviour).

In order to understand the behaviour of water better, a model using endless tubes for cells (axons), in which diffusion speed, permeability of the membrane and cell concentration was established and the results compared to measured DW-MRI data and results from a previous study [26]. For the estimation of the behaviour of water in areas with diffusion restriction a computer simulation was developed. A first model, based on axon models from previous studies, to analyse the importance of the diffusion hindering cell membrane on the measured non mono-exponential signal intensity decay was simulated. Ignoring the nearly non-existing exchange rate between extracellular and intracellular water pools, each pool could be studied separately. For this second step of simulations the first model, specially the starting conditions, had to be adjusted. The simulation data for the extracellular simulations also keeps information on the tortuosity changing effects of probably existing substructures. In

order to validate the simple models, the effect of randomly changing cell diameters with constant average diameter was investigated.

As the fitting of a bi-exponential function is sensitive to noise for estimation of the slow diffusion pool, another fit using diffusional kurtosis imaging (DKI) was applied. It had to be shown, that the fitted parameters are related to the underlying structure and that the parameters can be identified. The earlier mentioned models where used to identify the parameters, as effects like permeability and tortuosity in the extracellular space, caused by cell concentration, are impossible to calculate analytically and changing single parameters in physiological tissue for parameter identification is impossible. Also optimal b-values for DKI had to be evaluated, as that method uses a second order Taylor series, which was developed at $b = 0$ and therefore has a systematically error for higher b-values. Preview studies reported, that b-weighting with a maximal b-value below $2 \cdot 10^9 s \cdot m^{-2}$ results in parameter fits with too high standard derivation for precise fits. Thus, the b-weighting has to be optimized for lowest standard derivation with lowest methodical error caused by the Taylor series approach.

1.2 Motivation and Practical Relevance

There is a significant number of diseases that are said to be related to the damage of the blood-brain barrier (BBB), which result in an increased permeability of the vascular walls. In this case blood fluid and possible toxic substances can enter the brain causing inflammations and tissue abnormalities. What triggers these diseases is yet to be identified but the resulting lesions are detectable with means of diffusion weighted magnetic resonance images (DW-MRI). The best known of these diseases are multiple sclerosis (MS), Alzheimer's disease and HIV encephalitis. Drugs (like cocaine or extacy) can also cause a breakdown of the BBB. Furthermore, cerebrovascular diseases can damage the cerebral tissue directly and the BBB seriously. According to the World Health Organization (WHO) cerebrovascular diseases are

among the two leading death causes of cardiovascular diseases (Figure 1.1)[48] with 9.7% of total death in 2004 [49].

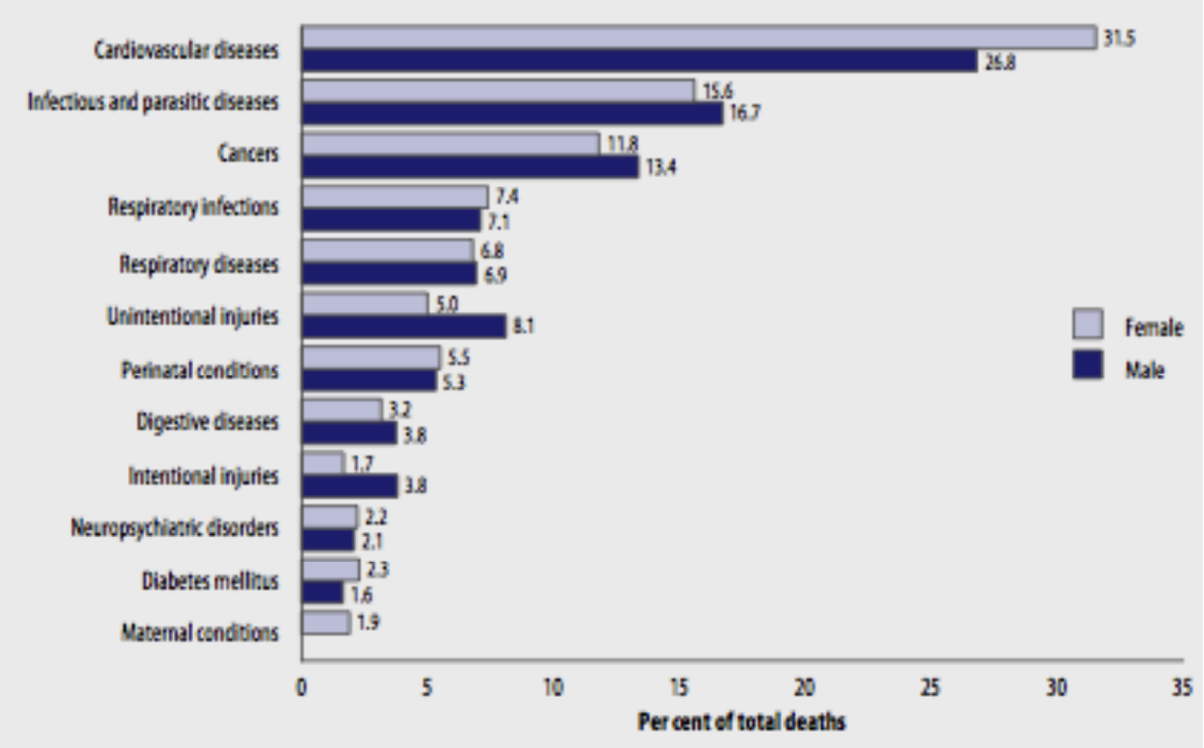

Figure 1.1: Distribution of deaths by leading cause groups, males and females, world, 2004. By WHO [48]

A series of studies has shown, that diffusion weighted images of biological tissue have a non mono-exponential signal decay. Thus a bi-exponential fit was introduced, with diffusion coefficients mapped to two different water pools, which are either said to be in the intracellular and extracellular space or only bound and bulk water (which is in both extracellular and intracellular volume). It is unclear which of the two to four pools are actually measured and how important the cell membrane is for the water movement. One of the main problems of the bi-exponential fit is the reduced signal to noise ratio (SNR) for the fit of parameters for the slow diffusion pool. Therefore a new approach had to be found. Assuming there is only one diffusion pool with non Brownian diffusion, measured data was compared to the Gaussian distribution using the second and forth central moment of probability, called diffusional kurtosis imaging (DKI). This approach satisfies the model of

two or more diffusion pools with Brownian diffusion and the higher SNR for the most noise sensitive parameter, because a fit with lower diffusion weighting is possible.

The relation of the DKI parameters and the underlying physiological tissue is still unclear. But it is well documented that the DKI-method has a methodical error when using high diffusion weighting.

For a precise interpretation of the measured data the answer to following questions seem to be crucial.

- What role does the cell membrane play for the measured diffusion data?
- Is it possible to identify the properties of the underlying tissue by means of the DKI parameters?
- If so, which parameters represent certain changes of tissue?
- What are the optimal b-values for DKI?

Early identification or risk detection of diseases gives the possibility to slow down symptoms of the disease by means of conventional treatments. Better understanding of the physiological tissue can lead to new and more effective future treatments.

1.3 Theses Objectives

The DKI parameters, apparent diffusion coefficient (ADC) and apparent kurtosis coefficient (AKC), are identified by use of self-programmed simulations based on cell geometry and permeability of the cell membrane. These simulations are also used to clarify the importance of the cell membrane in the process of water diffusion.
For data verification the simulation results were compared to studies form other institutions and diffusion weighted images recorded by GRAPPA method.
As the DKI approach uses a second order Taylor series, which is developed around $b = 0$, the used b-values should be as small as possible. But several studies have shown, that due to the noise, it is crucial that the highest b-value is at least $2 \cdot 10^9 s \cdot m^{-2}$. For the estimation of the optimal b-values the same images as for data verification were used.

2 Theory

2.1 Cerebrovascular Diseases

Cerebrovascular diseases are part of the cardiovascular diseases [48] and include all disorders in the brain area, which are transient or permanent effects caused by ischemia (in 80% of the cases [45]) or bleeding with one or more cerebral blood vessels involved. These diseases are caused by a restricted blood flow, which occurs in narrowing vessels (stenosis), clot formation (thrombosis), blockage (embolism) or blood vessel rupture (haemorrhage) and include strokes, stenosis, aneurysms and vascular malformations. The most common cause is hypertension, which causes damage to the walls of arteries and veins. The resulting lack of sufficient blood flow (ischemia) affects brain tissue and may cause a stroke.
The most common types of cerebrovascular diseases are [29]:

- Stroke, which is defined by the WHO as: "rapidly developing clinical signs of focal (or global) disturbance of cerebral function, with symptoms lasting 24 hours or longer or leading to death, with no apparent cause other than of vascular origin" [47].
- Transient ischemic attack (TIA) is a temporary fall in blood supply to the brain, resulting in ischemia for less then 24 hours (most symptoms resolve in a few minutes).
- Subarachnoid haemorrhage is an uncommon cause of stroke, were blood leaks out of the brain's blood vessels near the brain surface.
- Vascular dementia, where blood circulation problems result in parts of the brain not receiving blood and oxygen

2.2 Transient ischemic attack according to [37, 42]

TIA or “mini stroke” is a temporary cerebrovascular event with reduced perfusion to a local region of the brain causing a short disturbance of function. The difference between TIA and a stroke is, that TIA by definition resolves on its own (within 24 hours) while a stroke is permanent (symptoms last more than 24 hours). Recently, however studies from many groups worldwide have demonstrated that this arbitrary time threshold was too broad because classically defined TIAs also show brain injury on diffusion-weighted MRI (Table 2.1)[39]. The causes for TIA are the same as for stroke:

- A thrombus can form in one of the tiny arteries of the brain, which is normally preceded by gradual stenosis consisting of fatty build-up called plaque. Atherosclerosis (atheroma = deposits of cholesterol and fatty tissue + sclerosis + narrowing) of brain arteries is similar to the behaviour in heart arteries, which lead to heart attack. A blood clot can form if the plaque ruptures, leading to further blockage of the artery (embolism).
- An embolism can also occur if a thrombus is built in the heart and is transported to small arteries in the brain. Atrial fibrillation is the most common reason for an embolus, because it allows blood to become stagnant and form small clots. These cloths can embolize to any organ in the body, especially the brain proves to be a common target.
- Debris can occlude the blood vessels and stop the flow. This debris often breaks off from carotid arteries that are narrowed by atherosclerotic disease process described above.
- Blood vessels can leak and cause bleeding within the brain tissue. An intracerebral haemorrhage is often caused by high blood pressure. The resulting stress in the walls of small blood vessel can make them thin and weak.

If the mentioned causes are resolved fast, the ischemic tissue loses function for a short time, but doesn’t get permanently damaged. If the blood supply stays reduced for a few minutes, cell death occurs and leads to permanent neurological deficits.

Duration of Symptoms, h	DWI Hyperintensity
0–1	33.6
1–2	29.5
2–3	39.5
3–6	30.0
6–12	51.1
12–18	50.0
18–24	49.5

Table 2.1: Frequency of DWI abnormality in patients with transient neurological episodes of different duration. The data is from 10 MRI studies enrolling 818 Patients. Table is from [39].

Although the symptoms of TIA are the same as for a stroke the duration is different. Most of the time, they disappear after 1 hour but can last up to 24 hours.

- Neurologic deficits appear suddenly and can affect the ability to move or feel in one side of the body.
- Speech and vision can be affected.
- The affected person may experience confusion including a difficulty saying words or to follow orders.

Due to the brain being a large organ, only a part of the side may be affected. Symptoms can be limited to an arm or leg or part of the face. The deficits are also group based on the anatomy of the brain. For example, loss of speech, which is controlled by the left side of the brain, and weakness on the right side of the body are associated. These symptoms are associated with problems in the anterior circulation from the carotid arteries. The effects can vary from a large obvious neurotic defect like paralysis to something subtle like numbness or burning of a limb.

If the cerebellum is affected, the symptoms are much different and include:

- Dizziness
- Loss of balance and coordination
- Trouble walking

TIA to the base of the brain may result in drop attacks, in which the patient falls without warning.
Amaurosis Fugax is a specific type of TIA. An embolus in the ophthalmic arteries stops the blood supply of the retina, which causes sudden loss of vision in one eye and finally resolves spontaneously.

The diagnosis of TIA is often made by history, since the neurologic deficits have often resolved before the patient appears for care. This history may have information to identify the risk factors for heart disease, stroke and future TIAs:

- High blood pressure
- High colesterol
- Diabetes
- Smoking
- Family history

TIA is an indicator for increased risk of a future stroke (10% of the people with a TIA have a stroke within three months).

2.3 Diffusion and Self-Diffusion

Diffusion is the process of random molecular motion of the system. It was first recognized by Fick in 1885, who described the phenomenon in analogues to the transfer of heat by conduction. Fick's first law of diffusion stats that the flux is proportional to the local concentration differences in solute concentration, causing flux of matter from the area of higher concentration to ones with lower concentration. He also showed that, this flux changes the concentration C depend on the second spatial derivation of the concentration C and a constant D. This relation is known as Fick's second law of diffusion.

$$\frac{\partial C}{\partial t} = D\frac{\partial^2 C}{\partial x^2} \tag{2.1}$$

Self-diffusion or translational displacements of molecules is the random movement of molecules without a concentration gradient caused by the inner energy of a system as a consequence of Brownian motion, which is named after Robert Brown, a botanist, who observed the movement of plant spores floating in water.

Einstein [16] formulated a diffusion equation for Brownian movement in which the diffusion coefficient is related to the mean square displacement of a Brownian particle. He showed that $p(x,t)$ is the probability density function (PDF) of Brownian particles at a point x and a time t, if p satisfies the diffusion equation (substituting C with p). Assuming the diffusion starts at the point $x_0 = (0,0,0)$ and the time $t_0 = 0$ the solution is:

$$p(x,t) = \frac{1}{\sqrt{(4\pi t)D}} \cdot e^{\frac{-x^2}{4Dt}} \tag{2.2}$$

Mathematically, Brownian motion follows a Gaussian distribution with zero mean. This is related to the random walk model and is associated with stochastic processes (Wiener process) with normal distributed, independent increments of displacement.

The simplest random walk can be described by an initial position and a constant displacement ε with a random direction. After a constant time interval τ there is a collision and a new step is made from that point. After n steps the random displacement is possible to be calculated by a mean square distance $\langle R^2 \rangle$ in a given time t as a function of ε.

$$\langle R^2 \rangle = n\varepsilon^2 = \frac{t}{\tau}\varepsilon^2 \tag{2.3}$$

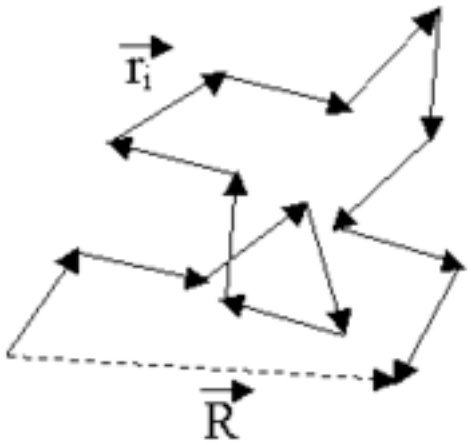

Figure 2.1: Random walk model to simulate Brownian motion.

You can also describe the diffusion by the probability that one particle has moved from position r' to a position r'' in a given time t. Where the probability $P(r'|r'',t)$ is proportional to the concentration at that point after the same time, if instead of one particle a lot of particles would have started in that point. And with:

$$R = (r'' - r') \tag{2.4}$$

The equation of Fick's second law of diffusion, in the simplest case of isotropic unrestricted self-diffusion, can be written as:

$$\frac{\partial P(R,t)}{\partial t} = \nabla^T \left(D \nabla P(R,t) \right) \tag{2.5}$$

The solution for the square dynamic displacement, $\langle R^2 \rangle$, can be expressed in terms of D for the three dimensions:

$$\langle R^2 \rangle = \int_{-\infty}^{\infty} R^2 \cdot P(\vec{R},t) d\vec{R} = 6Dt \tag{2.6}$$

and one dimension:

$$\langle (R_x)^2 \rangle = \int_{-\infty}^{\infty} R_x{}^2 \cdot P(R_x,t) dR_x = 2Dt \tag{2.7}$$

which shows, that the diffusion coefficient D_i, with i being the index of the unity vector in that diffusion direction, is the same as the diffusion coefficient D in this simple case. Also

the variance of the diffusion for three-dimensional problems is the sum of the 3 variances in orthogonal direction.

$$\left\langle R^2 \right\rangle = \left\langle R_x^2 + R_y^2 + R_z^2 \right\rangle = \left\langle R_x^2 \right\rangle + \left\langle R_y^2 \right\rangle + \left\langle R_z^2 \right\rangle \tag{2.8}$$

This shows that the diffusion in each direction is completely independent from the diffusion of the other two directions making it possible to calculate the effects on each direction separately and than add the results.

The self-diffusion coefficient for isotropic unrestricted diffusion in three dimensions is described by the Einstein equation [16]:

$$D = \frac{\xi^2}{6\tau} \tag{2.9}$$

The diffusion coefficient in an isotropic unrestricted matter is constant as long as the temperature is constant, too. The magnitude of movement for water caused by self-diffusion is extremely small, as the free diffusion coefficient for water at 25ºC is $D_{free}(25°C) = 2.27 \cdot 10^{-9} m^2 s^{-1}$ (pure water [44]) and calculated to be $D_{free}(37°C) = 3.05 \cdot 10^{-9} m^2 s^{-1}$ at 37ºC (pure water [19]). This is mainly caused by the viscosity change between 20ºC and 40ºC. The free diffusion coefficient at 37ºC would lead to an average displacement of 43 µm over a diffusion time of 100 ms.

2.4 Diffusion Measurement with MR-Techniques

Nuclear Magnetic Resonance (NMR) uses the fact that the magnetic quantum mechanical moment of the nucleus shows a specific behaviour in magnetic fields and that a magnetic field that rotates with the rotation speed of the magnetic moment (magnetic resonance) has the same effect as a static magnetic field on a static magnetic moment.

Self-diffusion measurement with NMR uses the fact that a moving spin in a gradient field has different magnetic resonance frequencies which causes the spin echo to be smaller than that of a none moving spin. This effect is used in the pulsed-gradient spin-echo (PGSE) sequence [41, 6].

2.4.1 Solution of the Bloch-Torrey Equation

Bloch equations [5] are a set of macroscopic equations to calculate the nuclear magnetization M as a function of time with the relaxation times T_1 (longitudinal) and T_2 (transversal).

$$\frac{\partial \vec{M}}{\partial t} = \gamma \vec{M} \times \vec{B} - \begin{pmatrix} 1/T_2 & 0 & 0 \\ 0 & 1/T_2 & 0 \\ 0 & 0 & 1/T_1 \end{pmatrix} \vec{M} + M_0 \begin{pmatrix} 0 \\ 0 \\ 1/T_1 \end{pmatrix} \tag{2.10}$$

M_0 is specified thermal equilibrium magnetization in the presence of a static magnetic field B_0. These equations where generalized by Torrey [43], who added magnetization transfer cause by diffusion with a self-diffusion coefficient (D).

$$\frac{\partial \vec{M}}{\partial t} = \gamma \vec{M} \times \vec{B} - \begin{pmatrix} 1/T_2 & 0 & 0 \\ 0 & 1/T_2 & 0 \\ 0 & 0 & 1/T_1 \end{pmatrix} \vec{M} + M_0 \begin{pmatrix} 0 \\ 0 \\ 1/T_1 \end{pmatrix} + \nabla^T \left(\vec{\vec{D}} \nabla \vec{M} \right) \tag{2.11}$$

For an imaging sequence a time depended gradient is added to the static main field B_0 resulting in a total magnetic field of:

$$\vec{B}(r,t) = \begin{pmatrix} 0 \\ 0 \\ \vec{G}(t) \cdot \vec{r} + B_0 \end{pmatrix} \tag{2.12}$$

With, r being the position vector and $\vec{G}(t)$ the added gradient:

$$\vec{G}(t) = \begin{pmatrix} G_x(t) \\ G_y(t) \\ G_z(t) \end{pmatrix} \tag{2.13}$$

Introducing a complex transverse magnetization M_T, which doesn't have a component in z direction, and equations (2.11 and 2.12) one obtains:

$$\frac{\partial M_T}{\partial t} = -i\gamma \left(B_0 - \left(G(t) \cdot r \right) \right) M_T - \frac{M_T}{T_2} + \nabla^T \left(D \nabla M_T \right) \tag{2.14}$$

The first term on the right side represents the static field and the gradient for the diffusion weighting. The second term is the T_2 decay caused by spin-spin-relaxation and the last term takes the diffusity into account.

Solving the equation (2.14) gives the time dependent behaviour of the transverse magnetisation M_T, which allows to study the diffusion mechanics on the magnetization in separate terms. Substituting the ∇-operator with $-j\vec{k}(t)$ the solution for the M_T in a magnetic field with only one gradient is:

$$M_T = M_T(0) \cdot e^{-iw_0 t - i\cdot\vec{r}\cdot\vec{k}(t) - \frac{t}{T_2}} e^{-\int_0^t \left(\vec{k}^T(t')\vec{\vec{D}}\vec{k}(t')dt\right)} \tag{2.15}$$

substituting

$$\int_0^t \left(\vec{k}^T(t')\vec{\vec{D}}\vec{k}(t')dt\right) = b\cdot D \tag{2.16}$$

M_T can be written as:

$$M_T = M_T(0) \cdot e^{-iw_0 t - i\cdot\vec{r}\cdot\vec{k}(t) - \frac{t}{T_2} - b\cdot D} \tag{2.17}$$

The first term is the rotation in the static magnetic field, the second term is the time dependent gradients, the third term is the spin-spin-relaxation and the last term is the diffusion mechanics.

Applying balanced gradients during an MR pulse sequence so both spin-echo and gradient-echo appear at the same time the signal, which is proportional to M_T is:

$$S(T_E, b) = C \cdot e^{-bD} e^{-\frac{T_E}{T_2}} \tag{2.18}$$

where C is the overall constant. $S(T_E, b)$ represents the signal for each voxel, which depends on it's diffusity and the spin-spin-relaxation time T_2 of the underlying tissue. Both T_E and b are linked with the used sequence and can be predefined by the use to get the desired signal. By varying only b one can achieve multiple b-weighted signals to calculate the diffusion.

$$\frac{S(T_E, b_2)}{S(T_E, b_1)} = \frac{C \cdot e^{-b_2 D} e^{-\frac{T_E}{T_2}}}{C \cdot e^{-b_1 D} e^{-\frac{T_E}{T_2}}} \tag{2.19}$$

$$\frac{S(T_E, b_2)}{S(T_E, b_1)} = e^{-(b_2 - b_1)D} \tag{2.20}$$

If the diffusion coefficient is linear with b the solution for diffusion coefficient D is as following:

$$D = \frac{1}{b_1 - b_2} \ln\left(\frac{S(T_E, b_2)}{S(T_E, b_1)}\right) \tag{2.21}$$

2.4.2 b-Value Notation

The b-value notation was introduced before (equation (2.16)). It represents the degree of diffusion weighting and therefore establishes a link between the measured NMR signal and the self-diffusion coefficient. It was first defined by Le Bihan et. al. (1986) :

$$b = \int_0^t \left(\vec{k}^T \cdot \vec{k}\right) dt' \tag{2.22}$$

with $k_x(t)$ being:

$$\vec{k} = \gamma \int_0^t G(t') dt' \tag{2.23}$$

The diffusion sensitizing depends on gradient's direction, strength and timing. The equation (2.23) also includes each imaging gradient. Even though the largest contribution to the b-matrix comes from diffusion sensitizing gradients, also the imaging gradients and "cross-terms" have to be taken into account. The effect of those cross-terms in diffusion imaging sequences have been discussed by Neeman et al. (1990), Matiello at el. (1997), Boujraf et al. (2001) and Brighuega-Moreno et al. (2004). If a high spatial resolution is wanted and diffusion weighting should be added, the dependence of imaging gradients and the diffusion weighting should be considered [18]. Most of the time the influence from imaging gradients on the b-matrix is low and neglecting imaging parameters and cross-terms leads to deviation of less than 3% [18].

2.4.3 Stejskal-Tanner Pulsed Field Gradient Sequence

Diffusion effects are extremely small and nearly invisible on conventional MR images. 1965 Stejskal and Tanner proposed a practical method to gain diffusion weighting by means of NMR technology. They used the well known, fundamental pulsed field gradient method

(PFG) to obtain signal attenuation due to water movement in a spin echo experiment. To do that, they used the fact, that a magnetic field gradient leads to different precision speeds and therefore the phase coherence is directly related to the gradient strength and duration. If a 180° pulse is used and the same gradient, symmetrically to the pulse, the spins which don't move are affected by the same gradient and therefore the phase shifts are completely compensated. Only spins that move are in a magnetic field with different strength during the second gradient and their phase shifts don't neutralize. As a consequence we can say, that if all spins move the same distance and direction, the change in the magnetic field strength during the gradient is the same for all spins and with that the phase change. This means uniform motion cannot be measured by means of magnitude imaging as a constant phase shift will cause no magnitude attenuation. But in water diffusion, where movement speed and direction are completely at random, the fact that phase changes are directly related to the moved distances and direction leads to different phase changes and the macroscopic magnetic vector, which is the sum of the magnetic spins, will be smaller. This signal intensity attenuation can be directly mapped to the diffusion.

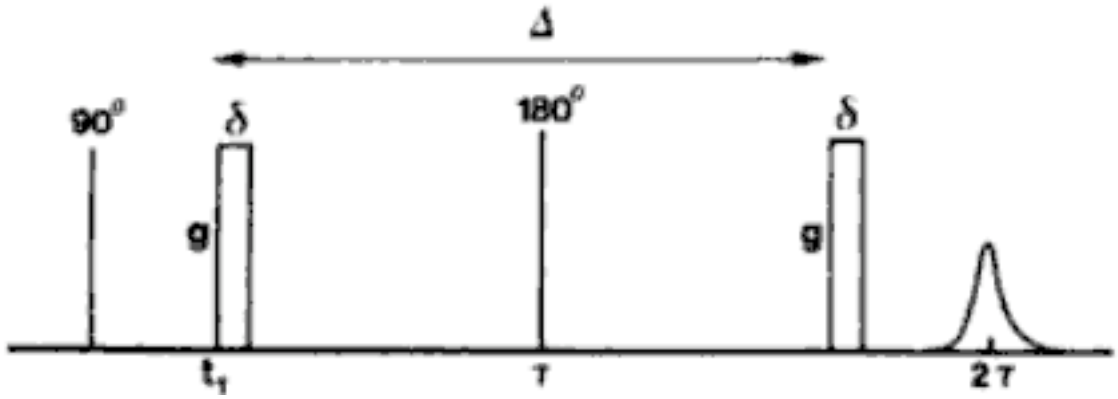

Figure 2.2: Basic Stejskal-Tanner pulsed gradient spin-echo (PGSE) pulse sequence used for displacement spectroscopy. The echo time is 2τ and the displacement time is Δ. Figure is from Bart [21].

2.5 Physiologically Reduced Diffusion

The biological tissue doesn't really affect the self-diffusion coefficient, but by means of boundary conditions the coefficient seems to be altered. This is way the term apparent diffusion coefficient (ADC) was introduced. Self-diffusion is a random Brownian motion with Gaussian distributed diffusion distance. This means the kurtosis excess is zero. If the diffusion is different from the Gaussian distributed diffusion distances, we can measure a kurtosis excess different from zero. The reasons for the appearance are discussed later, but similar to the ADC the term apparent kurtosis coefficient (AKC) was chosen.

2.6 Water Diffusion in Biological Tissues

The ADC of water in the brain is two to ten times lower than the unrestricted self-diffusion of water (which is $3.05 \mu m^2 \cdot ms^{-1}$ at 37ºC [19]). Higher viscosity, macromolecular crowding and diffusion hindering structures have been proposed to be the reasons for reduced water diffusion in the intracellular space [20], and tortuosity effects for the extracellular space [32, 12]. Restricted diffusion limits the water movement at the boundaries. If the boundary distance is larger compared to the average diffusion distance during the time of measuring this has no significant effect on the result. But in case of axons, where the water movement exceeds the axon radius, boundaries play an important role. Restriction can lower the diffusion coefficient in the intracellular space to values as low as 33% of the unrestricted diffusion. As you can easily see in the following formula for diffusion considering two ADCs are much smaller than the third. The additions of the diffusion coefficients in that way is easily described by the fact, that there are the orthogonal noise like signals with the ADC being proportional to their variances.

$$\langle ADC \rangle = \frac{ADC_x + ADC_y + ADC_z}{3} \tag{2.24}$$

The extracellular volume has also a lowered diffusion coefficient but it's dependent on the ratio between extra- and intracellular volume as its diffusion would also be hindered in two of

three directions. However, no clear restriction behaviour has been observed in vivo for water in the brain [7, 28]. Furthermore, studies established that the overall low diffusivity of water in cells can not be fully explained by compartmentation effects caused by the cell membranes or tortuosity from cellular macromolecules [37, 11, 15]. This strongly suggests that much smaller cellular components than those currently held responsible in MRI are the reason. In summary, the cell membranes in the brain cannot be the only reason for the reduced water diffusion. A recent research project shows that the cell membrane seems highly permeable, either passive or by means of transport, such as the specific aquaporin channels [3].

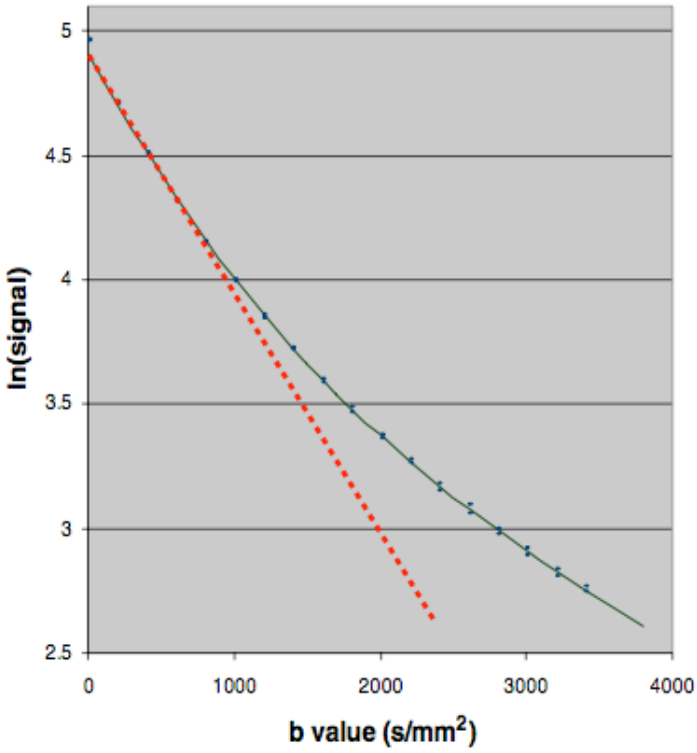

Figure 2.3: The red curve shows a mono-exponential signal intensity decay. The black curve shows the actually measured behaviour. Figure is from Bihan [9].

Many studies have experimentally established that diffusion-sensitized MRI could not be well described by a single exponential signal intensity decay, as it is the case in unrestricted, homogeneous medium (free Brownian diffusion) [7]. Furthermore, diffusion using the ‘q-

space' approach for data gathering showed a diffusion process, that cannot be modelled by a single Gaussian distribution [14].

Bi-exponential functions fitted the intensity decay well [34, 4].

$$S = S_0 \cdot \left(f_{slow} \cdot e^{-b \cdot D_{slow}} + f_{fast} \cdot e^{-b \cdot D_{fast}} \right) \tag{2.25}$$

where S_0 is the signal without diffusion weighting and includes the signal loss due to T_2-weighting of the signal caused by longer echo times because of the diffusion, f_{slow}, D_{slow} the slow water signal fraction and diffusion coefficient and f_{fast}, D_{fast} the fast water signal fraction and diffusion coefficient.

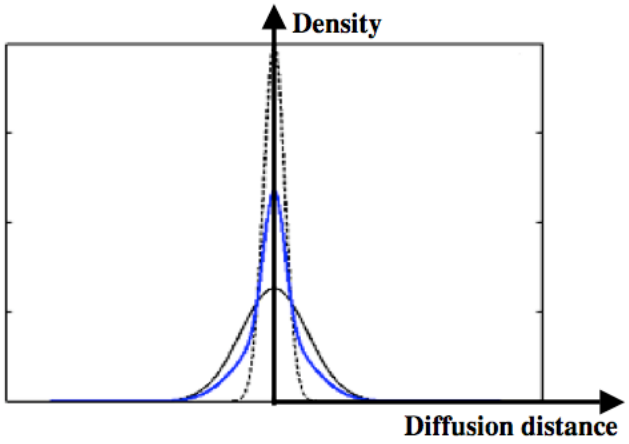

Figure 2.4: The bi-exponential fit assumes two Brownian diffusion pools with different standard derivations that together result in the blue non-Gaussian distributed random way. Figure is from Bihan [9].

Without T_2-relaxation:

$$f_{slow} + f_{fast} = 1 \tag{2.26}$$

This signal decay can be generated by two water pools with different diffusion coefficients and a slow exchange rate between these pools, or one non-Gaussian diffusion pool.

Diffusional kurtosis function can also be used and has a pretty good fit for low diffusion weighting and a systematic error that increases with higher b-values (second order Taylor series).

$$S = S_0 \cdot e^{-b \cdot ADC + \frac{b^2 \cdot AKC \cdot ADC^2}{6}} \tag{2.27}$$

With the bi-exponential fit the fast diffusion pool is about 70% of the signal and has a diffusion coefficient of around $D_{fast} = 1.27 \cdot 10^{-9} m^2 s^{-1}$ and the slow diffusion pool with about $D_{fast} = 0.27 \cdot 10^{-9} m^2 s^{-1}$ [9]. Compared to the extracellular volume fraction which is $f_{extra} \leq 0.15 \ldots 0.3 (0.2)$ (values are from different animals and different areas and without myelin fraction, which is considered as intracellular in that study. The value in brackets is from monkeys cerebral cortex) [32], it's questionable if fast and slow diffusion pools can be fitted to extracellular and intracellular volumes. Even if the different T_2-relaxation times are taken into account, the nature of these phases has remained unclear. A study using *Xenopus* oocytes, as the diameter is 1 mm and therefore exceeds the diffusion distance, provides that the diffusion in the intracellular volume, at least in these cells, have Brownian diffusion with about half the diffusion speed of free water [38]. This contradicts some previous studies which said before that in both intracellular and extracellular space bi-exponential signal intensity decays occur. Furthermore, theoretical models have shown that cylindrical membrane models generate pseudo bi-exponential diffusion behaviour [40]. Although these models might be able to simulate diffusion behaviour of WM it remains unclear if they can be applied for the cortex.

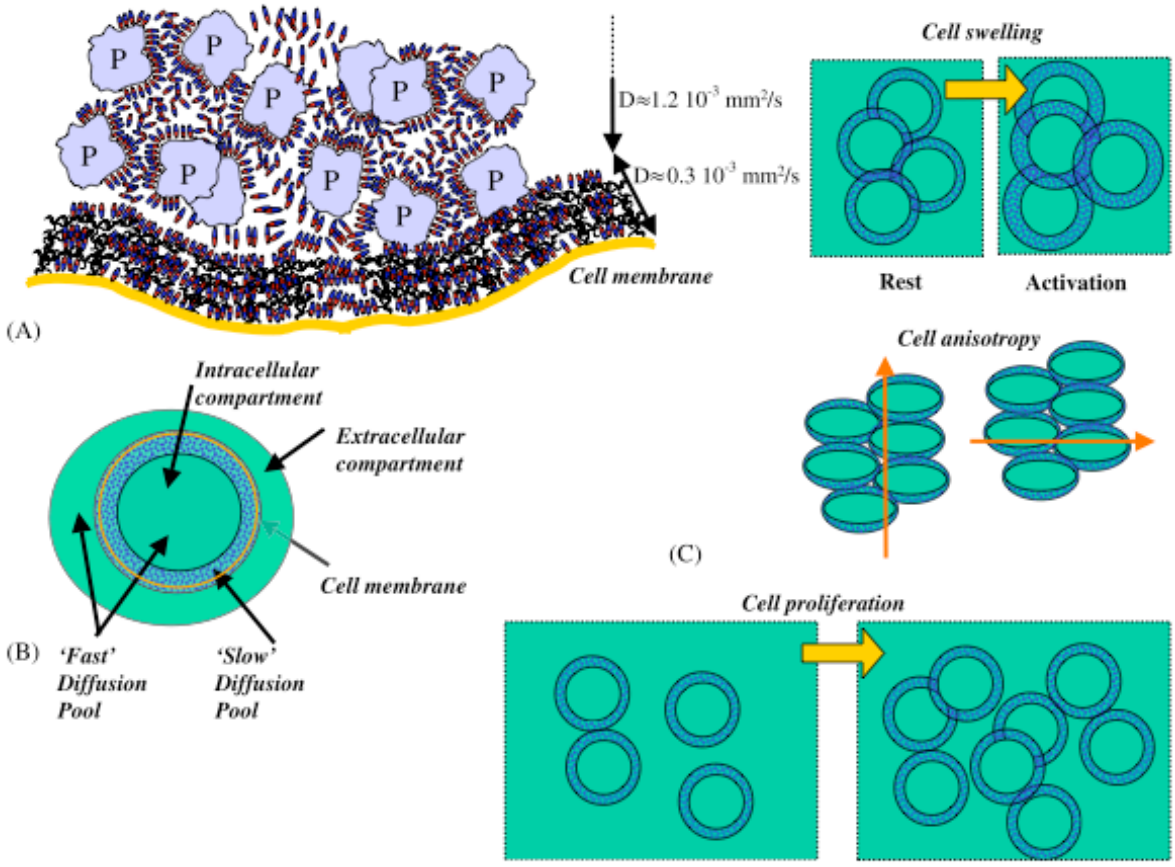

Figure 2.5: Membranes, water structure and diffusion. (A) Schematic representation of the structuring effect of proteins and membranes on water molecules (Bound water fraction). (B) Conceptual biphasic water diffusion model with bound water and bulk water fractions in the intracellular and extracellular space. (C) Variation of the bound water pool related to some changes of the cell membrane. Figure from Bihan [9].

2.7 Water Diffusion in the Extracellular Matrix (ECM)

The ECM and cell-membrane cause the water to take a longer way between two points and therefore decrease the ADC of water in the extracellular space. This apparent decrease of diffusity can be described by the tortuosity (λ). The easiest estimation of the tortuosity is:

$$\lambda = \frac{L}{C} \tag{2.28}$$

Where L is the actual way length and C the shortest way between starting point and ending point. This parameter can also be used for the intracellular volume to estimate the substructure of bound water and cell organelles. For case C is best estimated by the cell diameter in axial direction instead of the actual distance between two points, as this is the largest distance a water molecule can possible move and it provides a better information about the structure. For diffusion the average path length L can be calculated by the sum of all possibility weighted paths between two points. This calculated average length is compared to the shortest distance C between the two points ignoring all restrictions. With equation (2.28) the tortuosity can be defined as:

$$\lambda = \frac{\sum_{i=0}^{N} p_i \cdot L_i}{C} \tag{2.29}$$

with:

$$D_{free} = K \cdot \sum_{i=0}^{N} \left(p_i \cdot L_i \right)^2 = K \cdot \left(\sum_{i=0}^{N} p_i \cdot L_i \right)^2 \tag{2.30}$$

and:

$$ADC = K \cdot C^2 \tag{2.31}$$

The tortuosity as a function of the ADC is:

$$\lambda = \left(\frac{D_{free}}{ADC} \right)^{0.5} \tag{2.32}$$

Which is only correct if the tortuosity is the only reason for a slower diffusion (Figure 2.6).

Newer definitions for tortuosity take into account, that actually the change of the twist directions, reduces the actual diffusion speed. Which results in tortuosity definitions, which are zero for straight movement and motion in a circle [35, 25]. These newer definitions aren't useable for MRI as it doesn't make a difference if the diffusion is lowered by the fact that the twist direction changes or by the actual longer path that is needed to move a certain distance. This can easily be shown by the fact, the largest measured distance for the movement in a circle is the diameter of the circle and not the length of the path.

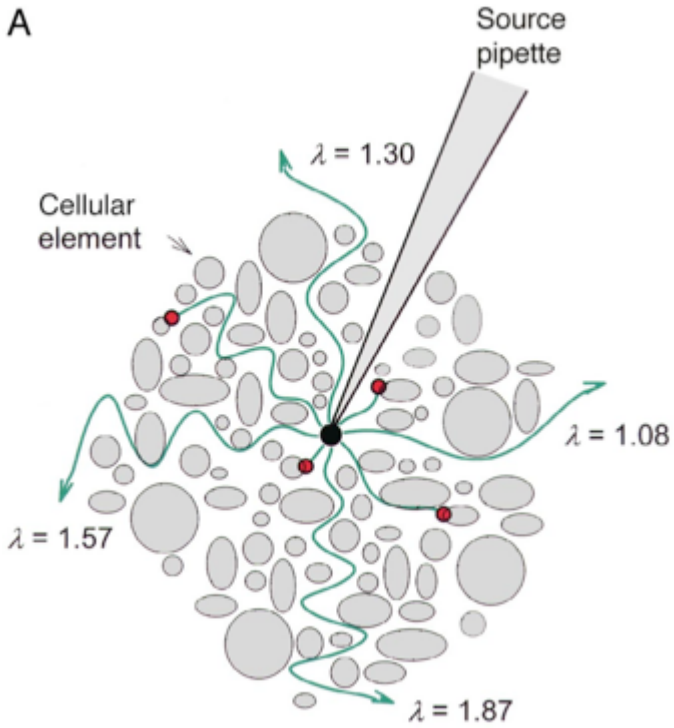

Figure 2.6: Tortuosity effects on the water diffusion in the extracellular space. Figure from Nichoslson [32]

For assumption of the extracellular substructure, the behaviour during ischemia gives information, as the fraction decreases to $f_{extra} \leq 0.04$ [32] which is only 20% of the normal value.

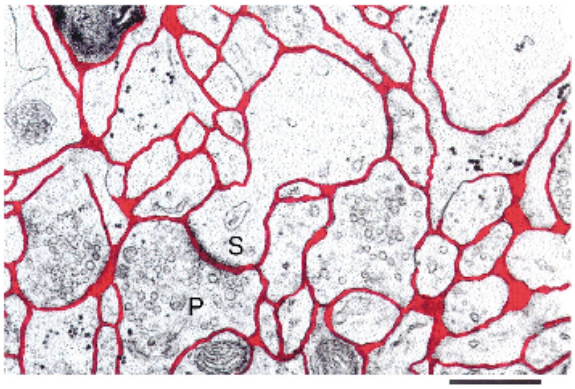

Figure 2.7: The red marked part is the extracellular space without the myelin sheath. The scale bar is $1\mu m$. With this marked images the ratio between extracellular space and intracellular space was estimated (note that the fixation might have changed the ratio). Figure from Nicholson [32].

2.8 Diffusional Kurtosis Imaging (DKI)

DKI is used to estimate the ADC and excess kurtosis (normally referred to as kurtosis in DKI) which is a dimensionless measure of the deviation between water diffusion and the Gauss distribution. The kurtosis can be caused either by measuring the diffusion distribution of two or more diffusion pools or one diffusion pool with non-Brownian diffusion.

2.8.1 Kurtosis and Excess Kurtosis

Kurtosis is the forth standardized moment of a probability distribution and is therefore defined as the forth central moment divided by the second central moment squared.

$$AKC(\Delta) = \frac{\left\langle (\vec{n}\cdot\vec{s})^4 \right\rangle}{\left\langle (\vec{n}\cdot\vec{s})^2 \right\rangle^2} \tag{2.33}$$

Where $AKC(\Delta)$ is the apparent kurtosis after the diffusion time (Δ) and ($\vec{n}\cdot\vec{s}$) the moved distance ($\vec{s}$) in direction ($\vec{n}$). It is a measure for the 'peakedness' of the distribution. The value of the normal distribution is three. If the distribution has a kurtosis that is higher than 3, it's peaked. If it's lower than three it's flat compared to the normal distribution. The excess kurtosis is the kurtosis minus three. Which results in distribution that is zero for Gaussian derivation and positive when it's 'peaked', which is the case in the human brain [17].

$$AKC(\Delta) = \frac{\left\langle (\vec{n}\cdot\vec{s})^4 \right\rangle}{\left\langle (\vec{n}\cdot\vec{s})^2 \right\rangle^2} - 3 \tag{2.34}$$

The apparent diffusion coefficient ($ADC(\Delta)$) is [17]:

$$ADC(\Delta) = \frac{1}{2\cdot\Delta}\left\langle (\vec{n}\cdot\vec{s})^2 \right\rangle \tag{2.35}$$

2.8.2 Taylor Series

A Taylor series is a representation of a function as an infinite sum of power terms.

$$f(x) = \sum_{i=0}^{\infty} \frac{f^{(i)}(a)}{i!}(x-a)^i \tag{2.36}$$

where $f(x)$ is the original function, a the point it's developed around. To reduce the calculation effort terms with higher powers can be ignored, as they normally hold less information about the function near the point it was developed. The highest power, is the order of the fitted Taylor series. The DKI uses a second order Taylor series, which is developed around the point $b = 0$, for the fit of the exponent of the MRI signal intensity decay. The normalised MRI signal is 1 at $b = 0$ which leads to a Taylor series without the first element as $\ln(1) = 0$.

$$\ln\left(\frac{S(b)}{S_0}\right) = \sum_{i=1}^{2} C_i \cdot b^i \tag{2.37}$$

where $S(b)$ is the signal at the diffusion weighting b and $S_0 = S(0)$. The relation between the coefficients of the Taylor series and the ADC and AKC are as following [17].

$$C_1 = -ADC \tag{2.38}$$

$$C_2 = \frac{AKC \cdot ADC^2}{6} \tag{2.39}$$

which leads too:

$$\frac{S(b)}{S_0} = e^{-ADC \cdot b + \frac{AKC \cdot ADC^2 \cdot b^2}{6}} \tag{2.40}$$

As the Taylor series is second order the using of this function to fit the signal intensity decay for high b-values leads to a systematically error. Higher order series might give a better fit in these areas. But lower SNR and an additional parameter for fitting, might result in misinterpretation of the MRI data.

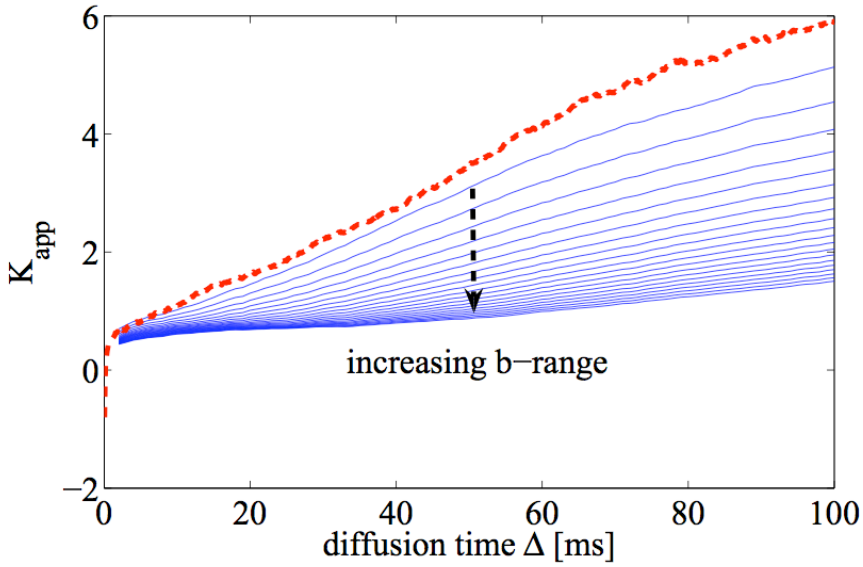

Figure 2.8: This figure shows the behaviour of the AKC for increasing b-values. The red curve is the fitted AKC with the following b-values $\left[0\ldots 0.5\cdot 10^{9}\, s\cdot m^{-2}\right]$ and the lowest blue curve is with the following b-values $\left[0\ldots 10\cdot 10^{9}\, s\cdot m^{-2}\right]$. Figure from Fieremans [17].

2.9 Magnitude Images and Image Noise

In magnitude images only the length of the magnetization vector is used for the generation of the image. This means, information about the phase is ignored, but that can't be the case for the calculation of noise like effects on the signal as both signals are complex signals and both the length and phase of the noise vector are unknown and at random. Consequently the complex noise and signal have to be added in the complex plane. Therefore the imaginary parts and real parts of both variables have to be added separately and than added geometrically for the calculation of the resulting magnitude.

$$\underline{S_{[u,v]}} = S_{R,[u,v]} + iS_{I,[u,v]} \tag{2.41}$$

$$\underline{N_{[u,v]}} = N_{R,[u,v]} + iN_{I,[u,v]} \tag{2.42}$$

$$\underline{S_{noisy[u,v]}} = N_{R,[u,v]} + iN_{I,[u,v]} + S_{R,[u,v]} + iS_{I,[u,v]} \tag{2.43}$$

where $[u,v]$ are the local variable of the voxel in the selected slice and the noise signal being a complex white noise which means Gaussian distributed with zero mean and σ as standard derivation. As only the magnitude is important for magnitude images, the complex plane can be rotated to eliminate the imaginary part of the noise free signal. The complex noise in the rotated coordinate system consists of the same average magnitude and an angle between the noise and the signal S.

$$\underline{N_{[u,v]}} = \left|N_{[u,v]}\right| \cdot e^{j\alpha_{[u,v]}} \tag{2.44}$$

with equation (2.43):

$$\underline{S_{noisy[u,v]}} = \left|N_{[u,v]}\right| \cdot e^{j\alpha_{[u,v]}} + \left|S_{[u,v]}\right| \tag{2.45}$$

Thus the magnitude can be written as.

$$\left|\underline{S_{noisy[u,v]}}\right| = \sqrt{\left(N_{[u,v]} \cdot \cos\left(\alpha_{[u,v]}\right) + S_{[u,v]}\right)^2 + \left(N_{[u,v]} \cdot \sin\left(\alpha_{[u,v]}\right)\right)^2} \tag{2.46}$$

As the magnitude is always positive, the negative root can be ignored. If the noise free signal has a much larger magnitude than the noise, the noise can be assumed Gaussian distributed with zero mean which allows to get a better signal to noise ratio by averaging. In all other cases the measured noise distribution can no longer be assumed Gaussian with zero mean as the signal is always positive and the average of the noisy magnitude is lager than the magnitude of the noise free data. The nonlinear mapping results in the following probability density function $p(M)$ [2] for the random variable M.

$$p(M;A,\sigma) = \frac{M}{\sigma^2} e^{-\frac{\left(M^2+A^2\right)}{2\cdot\sigma^2}} \cdot I_0 \cdot \left(\frac{M \cdot A}{\sigma^2}\right) \tag{2.47}$$

where $I_0(x)$ is the modified zeroth order Bessel function of the first kind and A the noise free signal intensity. This equation is commonly known as Rician distribution, proposed by Rice. If the standard derivation of the noise is much lager than the magnitude of the noise free signal, the Rayleigh (first considered by Lord Rayleigh in 1880) distribution satisfies the Rician distribution. This means the measured magnitude is mainly dependent on the noise.

$$\overline{M} = \sqrt{\frac{\pi}{2}} \cdot \sigma \approx 1.253 \cdot \sigma \tag{2.48}$$

$$\sigma_M^2 = \left(\frac{4-\pi}{2}\right)\cdot \sigma^2 \approx (0.655\cdot \sigma)^2 \tag{2.49}$$

As it can be seen the mean of the signal is slightly higher than the standard derivation of the Gaussian distribution the Rayleigh distribution is based on. This means only by averaging the noise effects cannot be eliminated anymore.

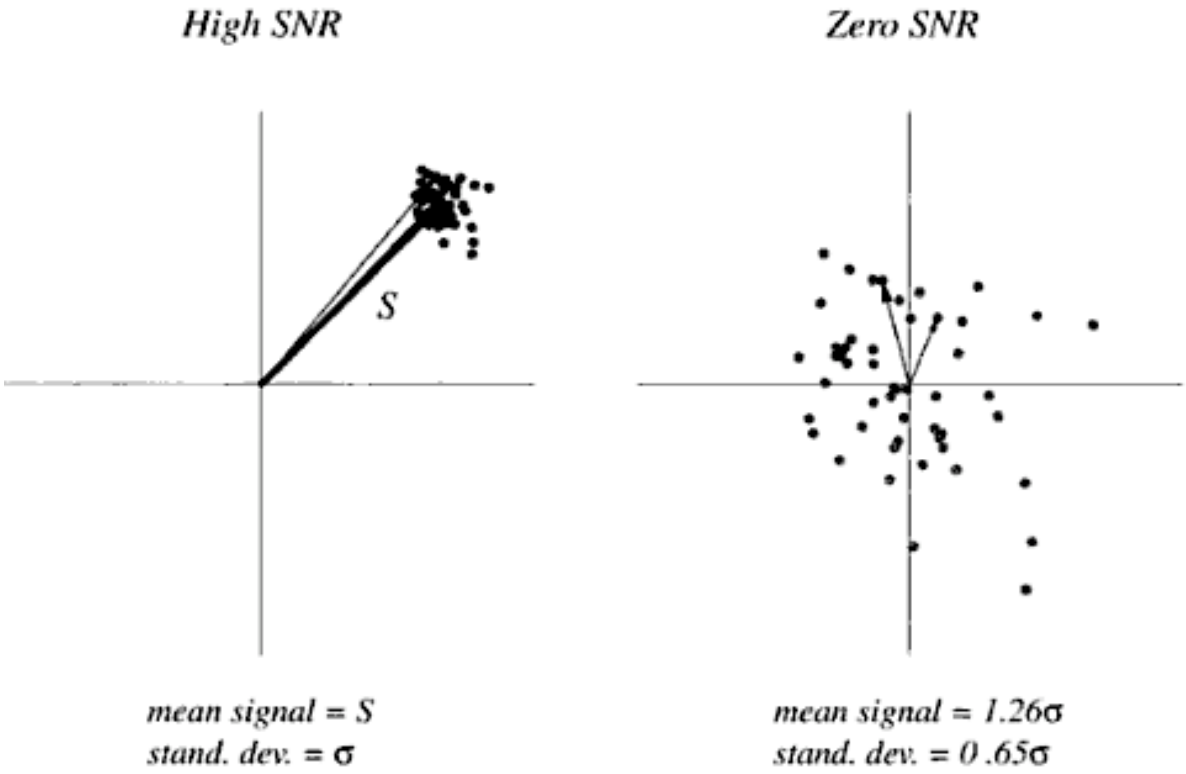

Figure 2.9: Effect of different SNR on the standard derivation and mean of the signal.

2.10 Signal to Noise Ratio (SNR)

The SNR is dependent on the actual signal magnitude and the standard derivation of the noise.

$$SNR = \frac{S}{\sigma_n} \tag{2.50}$$

If the noise is Gaussian the SNR can be increased by averaging.

$$SNR = \frac{S}{\sigma_n}\sqrt{N} \tag{2.51}$$

where N is the number of averages used.

If the measured noise is Rayleigh distributed, the standard derivation of the noise can be estimated with enough numbers of averages. If the diffusion weighting is high enough, the noise can be assumed for every measured voxel, or averaged for a few voxels close to each other. As with increase of diffusion weighting, the signal from moving water can be eliminated.

$$\frac{S(b=\infty)}{S(b=0)} = \frac{\overline{M}}{|S|} \approx 1.253 \cdot SNR^{-1} \tag{2.52}$$

$$SNR \approx 1.253 \cdot \frac{S(b=0)}{S(b=\infty)} \tag{2.53}$$

This means one higher b-value is important for noise estimation, because it can be assumed, that the increase of the averaged noisy signal at higher values has an impact on the fitted AKC.

3 Methods

3.1 Monte Carlo Methods

Monte Carlo Methods are a class of numerical methods, which use random values to approximate the true solution of a complex problem. The accuracy of the approach, increases with the number of random values that are used and reaches the true solution for an infinite number of random values. As the calculation effort also increases with a higher number of random values, this algorithm is stopped at a certain accuracy. The class of methods was named by S. Ulam in 1946.

3.1.1 Monte Carlo Integration

In order to integrate a function over a complicated domain D, Monte Carlo integration uses a simple domain D' which is a superset of domain D and randomly fills the area with points. The probability of the point being in D is the ration between D and D'. After evaluating how many points are in the domain D the integral can be estimated by:

$$\int f dD = \frac{N_D}{N} \int f dD' \tag{3.1}$$

where N_D is the number of points in D and N the total number of points.

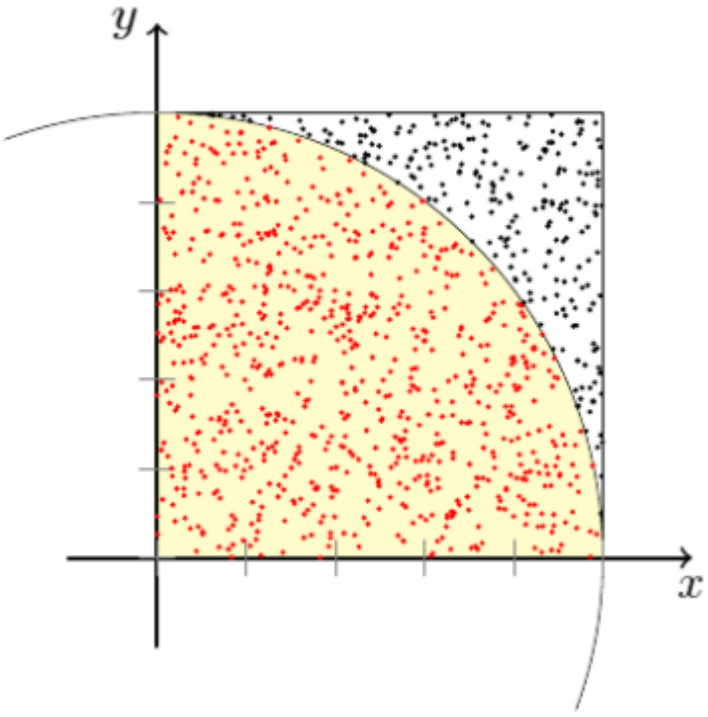

Figure 3.1: Approximation of π by means of Monte Carlo Integration ($\pi = \left(A_{curcle} / A_{square} \right) \cdot 4$).

3.1.2 Markov Chain Monte Carlo

Markov Chain Monte Carlo is a time discrete random process, that has no memory (meaning that future system states only depend on the current state, and not the possible past states) which is called the Markov property [1]. This also covers random walk Monte Carlo methods. Where the future position of a particle only depends on the current position and an estimation to calculate the vector between its current state and its next.

3.1.3 Random Walk

The two-dimensional random walk problem is easy to solve using a random walk Monte Carlo method based on the Markov chain [1]. The simplest probability distribution for each step, given a small enough step size, is:

$$p(x,y) = r\cdot\left(\cos(\varphi)e_x + \sin(\varphi)e_y\right) \tag{3.2}$$

With φ being the step vectors rotation angle that has the same likelihood for each value and $p(x,y)$ being the probability function that has the same likelihood for every position on a circle. As a result the random way distribution has the same variance in the orthogonal directions [24].

$$\sigma^2 = \int (u-u_0)^2 \tag{3.3}$$

$$\sigma^2 = \frac{1}{2\pi}\int_0^{2\pi}\sin^2(\varphi)d\varphi = \frac{1}{2\pi}\int_0^{2\pi}\cos^2(\varphi)d\varphi = 0.5 \tag{3.4}$$

The three-dimensional equivalent to the circle is a spherical surface.

$$p(x,y,z) = r\cdot\left(\cos(\varphi)\cos(\psi)e_x + \sin(\varphi)\cos(\psi)e_y + \sin(\psi)e_z\right) \tag{3.5}$$

Clearly the variances in the three directions aren't the same.

$$\sigma_x^2 = \left(\frac{1}{2\pi}\right)^2\int_0^{2\pi}\int_0^{2\pi}\cos^2(\varphi)\cos^2(\psi)d\varphi d\psi = 0.25 \tag{3.6}$$

$$\sigma_y^2 = \left(\frac{1}{2\pi}\right)^2\int_0^{2\pi}\int_0^{2\pi}\sin^2(\varphi)\cos^2(\psi)d\varphi d\psi = 0.25 \tag{3.7}$$

$$\sigma_z^2 = \frac{1}{2\pi}\int_0^{2\pi}\sin^2(\psi)d\psi = 0.5 \tag{3.8}$$

As the average variance in each direction should be $1/3$ ($\sigma_x^2+\sigma_z^2+\sigma_z^2 = 1 \ldots \sigma_x^2 = \sigma_z^2 = \sigma_z^2$) the surface will be deformed to generate an isotropic random walk.

$$p(x,y,z) = r\cdot\left(\sqrt{\frac{4}{3}}\cos(\varphi)\cos(\psi)e_x + \sqrt{\frac{4}{3}}\sin(\varphi)\cos(\psi)e_y + \sqrt{\frac{2}{3}}\sin(\psi)e_z\right) \tag{3.9}$$

The step size r is given by the Brownian motion (equation 2.9):

$$p(x,y,z) = \sqrt{6D\tau}\left(\sqrt{\frac{4}{3}}\cos(\varphi)\cos(\psi)e_x + \sqrt{\frac{4}{3}}\sin(\varphi)\cos(\psi)e_y + \sqrt{\frac{2}{3}}\sin(\psi)e_z\right) \tag{3.10}$$

where D is the diffusion coefficient and t is the time that passes between two steps.

3.2 Noise Sensitivity Estimation

To estimate the sensitivity of fits used to predict the underlying tissue, two different noise models were added to the simulation data. In a further step the resulting noisy signals were compared to the actual measured data and the effect on the fitted parameters compared to the pure simulation data.

3.2.1 Complex Noise

To simulate the effect of the random noise magnitude and the angle between noise signal and the vector of the transversal magnetic field, noise with a random angle and amplitude was added and the magnitude of the resulting vector was averaged.

$$f(b) = \sqrt{\left(s(b) + \cos\left(\alpha_{noise}\right)\cdot n\right)^2 + \sin^2\left(\alpha_{noise}\right)\cdot n^2} \tag{3.11}$$

where α_{noise} is the angle between the magnetization vector and the noise vector.

3.2.2 Offset

As a simple noise model an offset was added to the simulation data to fit the measured data as for high signal values the SNR is higher. The error made by this noise model, was rather low for low *b*-values while for low SNR the noise is similar to the noise in the complex noise model. Therefore a slightly too high effect of noise on the measured signal for mid-level *b*-weighting was assumed.

$$f(b) = s(b) + offset \tag{3.12}$$

3.2.3 Estimation of Parameter Noise Sensitivity

The parameters for DKI were fit with the data from the simulation and the noisy signals generated from the simulation data and compared with the actual diffusion and kurtosis of the simulation. In addition a bi-exponential fit was made for all 3 data sets and compared.

3.3 Comparison to Measured Data

The resulting noisy signals were fitted bi-exponential for a smooth curve to compare with measured data. And the signal intensity decays compared by means of diagrams. This method was used as differences between curves can be easily seen that way and the DKI approach has a significant error at high b-values. Due to this error a comparison in this area would have been impossible.

3.4 Evaluation of Optimal b-Factors

The probable SNR data from the noise estimation were used to estimate the maximum b-values, because a signal, that consists mainly of noise, doesn't give information about the underlying tissue, even if the fit is more robust using that data.
To estimate the minimum for the highest b-value, measured data was used to calculate the standard derivation of the fitted parameters in small areas with values close to $b = 0$, as it is most likely that under those circumstances the underlying tissue properties are similar.
The third method to estimate the optimal value for the highest b-weighting was the comparison of the parameters with the actual simulation values, as the DKI approach has a methodical error at higher b-values.

4 Software Realisation

4.1 Software and Framework

Matlab R2009b (developed by MathWorks Inc.) was used for the simulation of the axon models. This software was also used for noise simulation and the bi-exponential and diffusional kurtosis fits.
For MRI data achievement OsiriX v3.9.2 32 bit (LGPL) for MAC OS X was used.

4.2 The Simulation of the Axon Model

The model was based on commonly used axon model to simulate white matter. For a much simpler simulation the neurons in white matter can be modelled to consist only of axons. This is possible as the volume of the soma is rather small compared to the volume of the axon. In a second simplification the axons could be assumed indefinitely long as the length exceeds the diffusion length. These two simplifications allow the development of an effective two-dimensional simulation which significantly decreases the simulation effort.
As shown in a previous study [17] the bi-exponential and DKI parameters aren't significantly affected by the geometrical order. As a result a geometrical order could be used, that maximizes the minimal distance between two neighbouring axons. The order that satisfies this condition is a hexagonal structure.
To estimate the simulation area, the maximal diffusion distance possible had to be estimated.

$$r_{\max} = r_{\Delta t} \cdot \frac{T}{\Delta t} \tag{4.1}$$

The theoretical simulation radius needed (for a time step length Δt of $1\mu s$, a diffusion coefficient D of $2 \cdot 10^{-9} m^2 \cdot s^{-1}$ and a simulation time T of $100ms$) would be about $11 \cdot 10^{-3} m$ (This would mean around 10^8 axons for exact simulation. Even with the assumption that the standard derivation of the diffusion is $35\mu m$, a number of over 10^4 cell would have been needed.). This easily shows, that the diffusion area had to be imaginary expanded. This is possible by mirroring, both the starting point and the new point at the simulation border. This simple method mirrored the structure within the simulated area at each border for an infinite number of times. Thus the simulation area appeared to be endless. This simple trick allowed to actually simulate the whole diffusion with only 23 axons.

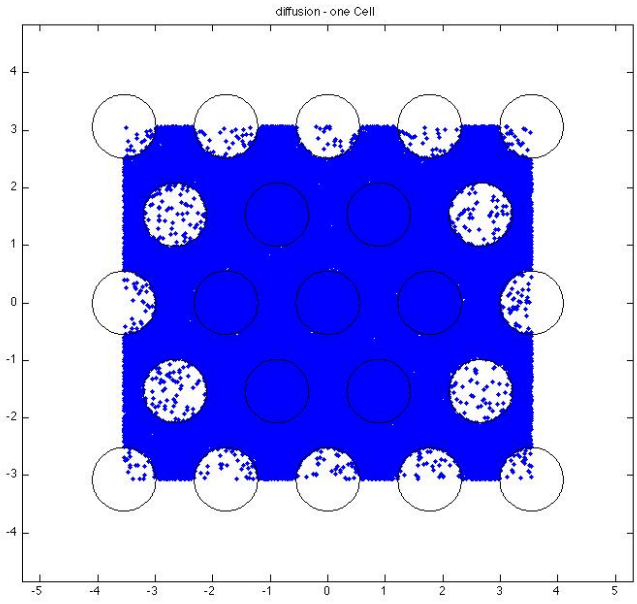

Figure 4.1: Implementation of the axon structure (symbolised by the circles with a cell concentration is 35% and membranes which let only 10^{-5} molecules that interact with them pass). The blue particles are water molecules after $100ms$ diffusion time.

For the random way generation a Markov Chain random walk model was used. The cell membrane and simulation borders were assumed to reflect the water molecules elastically.

The borders also reflected the starting points of the molecules elastically as mentioned above (the borders of the simulation can be seen in Figure 4.1 as it's also the border of the blue area.). The simulation code is in Appendix A.

In order to evaluate the effects of the *b*-values on the diffusion coefficient and on the kurtosis, the results of the random walk simulation were inserted into the Matlab algorithms for the calculation of the standard derivation and the kurtosis. A signal intensity curve calculated from the simulation data was also generated to be compared with measured data and to calculate the fitted parameters.

4.3 Noise Generation

The generated complex noise was Gaussian distributed with zero mean. It was added geometrically with the noise free signal magnitude. The standard derivation of the noise was varied constantly to estimate the effects of different SNRs on the fitted parameters of bi-exponential and DKI.
Offset like noise was also introduced. This noise had no imaginary part and was generated by using the magnitude of Gaussian noise with zero mean.

4.4 Validation of the Simulation Assumptions

For the validation of the simulation assumption of choosing the same diameter for the axons, the model was altered and the true parameters (both bi-exponential and DKI) were calculated and compared to the values of the simulation using the same cell concentration but varying cell diameters. To ensure the correct cell concentration after random radius generation the ratio between the extracellular volume and the intracellular volume was estimated using Monte Carlo integration. This was essential for this validation since a random variation of the cell concentration has an impact on the parameters. Without this test to correct the cell

concentration after randomly varying the axon diameters, the parameters had randomly changed in a small range compared to the simulation using the fixed axon diameters.

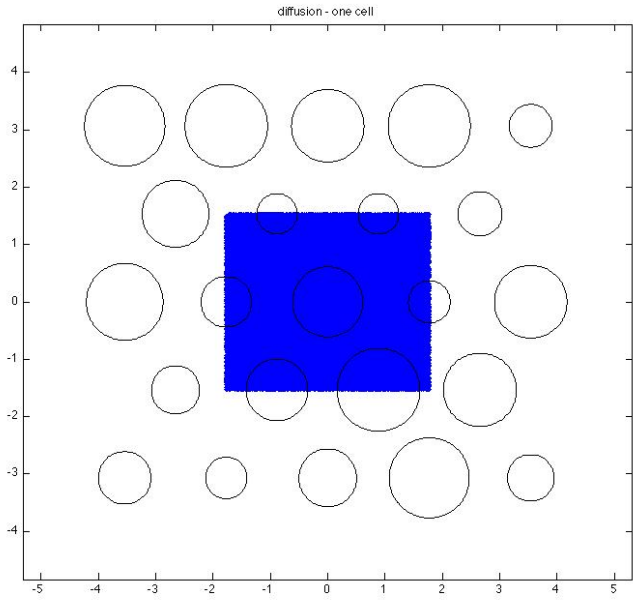

Figure 4.2: Axon structure to validate the simulation. The blue Area is the starting area of the simulated particles and the circles are the axons with random diameters with a cell concentration of 35%.

4.5 Comparison with Measured Data

The simulation parameters were altered to fit the measured data of a previous study [26]. This alteration was applied to prove that different cell membrane permeabilities can cause the AKC change between WM and GM (or to be more precise the myelination which was simulated as part of the membrane because of lower simulation effort).

The comparison to the measured data sets showed that the simulation using one “free” diffusion coefficient for both extracellular space and intracellular space could not be used to model the structural changes related to the change of cell concentration (excluding ischemic

effects, as the underlying structure can be assumed unchanged). Thus, the intracellular space and extracellular space were simulated separately and the results were used to estimate the underlying structure based on the T_2-weighted image (for substructures as well as cell concentration).

Matlab was used to generate signals based on the substructures and cell concentration with added noise effects. The model was altered based on the comparison between the predicted diffusion behaviour and the data of one healthy subject.

4.6 Validation of the Model

To validate the final model the diffusional behaviour of measured data from one healthy and ten pathological test subjects was compared to the predicted diffusion behaviours based on the model using Matlab (the SNR for the effects based by noise was taken by the average ratio between the T_2-weighted image and the diffusion weighted image with $b = 5 \cdot 10^9 s \cdot m^{-2}$).

5 Results

5.1 Simulations

All simulations and calculations were made under the assumption that all distances of the structures and substructures are large if compared to the size of a water molecule and the distance a water molecule moves within a *ns* (else a diffusion formula that includes quantum mechanical effects would have been needed). Also the structures were said to have no other significant effect on the diffusion coefficient than by reflecting the particles. This can be assumed, as diffusion is a slow process and therefore interaction between structures and water molecules can be estimated by the means of elastic collisions.

5.1.1 Water Diffusion in a Cell Cluster

The behaviour of water motion in a cell cluster is affected by a lot of different parameters. And it's hard to make precise distinctions on the water behaviour without a simulation, in which you can change single parameters without affecting any of the other parameters. This part concentrates on the effects caused solely by the cell membrane. The diffusion coefficients in the extracellular and intracellular space are assumed to be the same for easier simulation. The cell concentration, cell diameter and cell membrane permeability were changed constantly to evaluate the effect on the ADC and AKC.

5.1.2 Cell Cluster Simulation

For less simulation effort the cells where simplified to consist only of axons. The axons were assumed to be endless parallel tubes with the same diameters (the axial direction was in z direction and the radial direction in the $x - y$ plane). To verify the assumption of the same diameter for each cell, a few simulations were made with largely varying cell diameters, which didn't have significantly different results. This decreased the simulation complexity a lot, as only a few cells had to be simulated (the simulation effort is linked to the number of cells and therefore linear linked to the simulation area) and the cell cluster could be assumed to continue to infinity with the same parameters, which can be generated, by mirror like simulation borders (on each interaction, both starting point and new position were mirrored at the boundary).

For the simulation only the cell membranes and the movement of water was simulated. The cell membrane was a permeable membrane that has a set chance to let water pass through it. Water that didn't pass through the membrane was reflected elastically at its boundaries. The cell were set to be in a hexagonal structure, for this structure leads to the highest possible cell concentration, which enables the fastest simulation speed and concentrations that aren't possible with a quadratic array. Both the permeability and the concentration were variable parameters in this simulation.

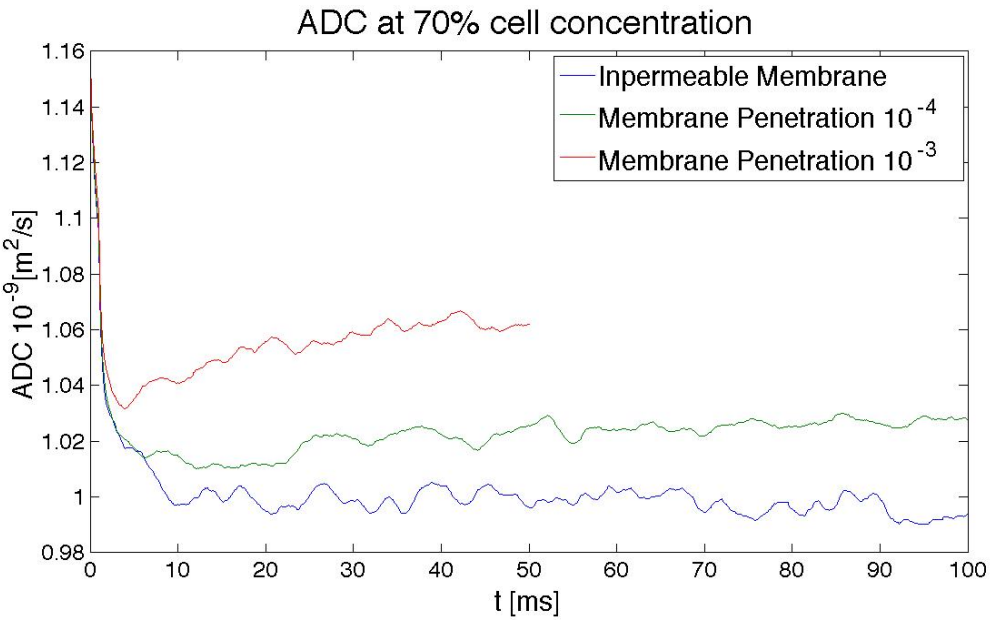

Figure 5.1: ADC change with variation of permeability of the cell membrane. It slightly increases for chances above 0.1%. As the AKC would vanish at that permeability, the ADC is not altered by change of cell membrane permeability.

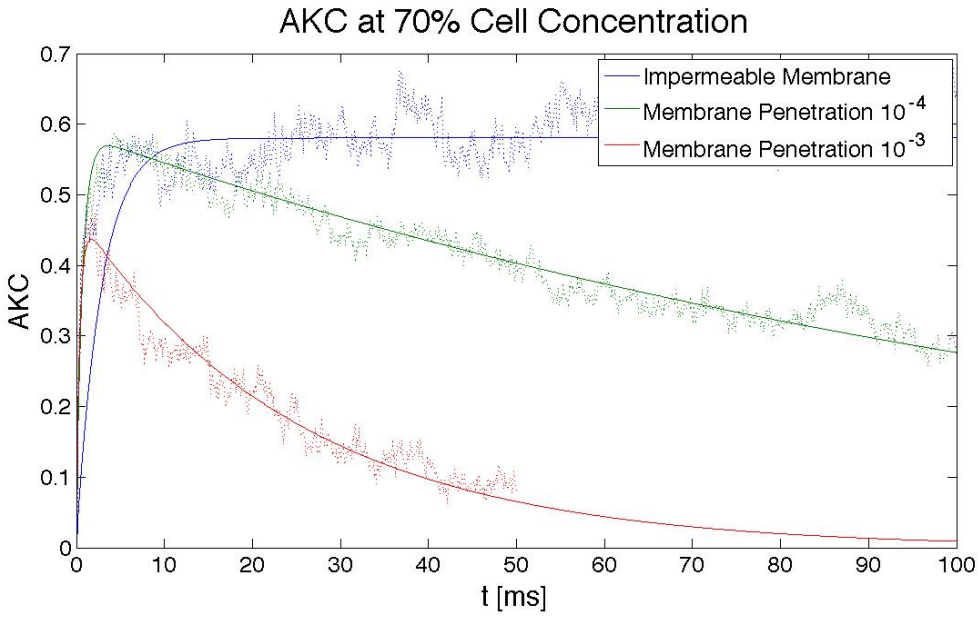

Figure 5.2: As seen here the AKC changes with diffusion time and permeability of the cell membrane. Thus the AKC can be used as an indicator for permeability changes of the cell membrane.

Changing the permeability of the cell membrane mainly affected the AKC. A change in the ADC (Figure 5.1) was not significant, till the AKC disappeared (at 0.1% diffusion chance through the membrane in less $50ms$ and with 1% in less than $10ms$). This lead to the assumption that any water pools which are responsible for the non mono-exponential signal intensity decay have to be separated by means of a highly diffusion hindering or completely restricting membrane. Otherwise the diffusion would lead to a measured mono-exponential signal intensity decay, because the exchange between the water pools would be fast enough to appear as only one water pool. Changing the permeability from 0% to 0.1% (10 ms diffusion time) at a concentration of 70% extracellular volume and a diffusion coefficient of $D = 2.1 \cdot 10^{-9} m^2 s^{-1}$ showed the same ADC for both cases and an AKC change that was similar to measured data between WM and GM [26]. As easily can be seen the DKI has a significant methodical error at high b-factors (Figure 5.3 and Figure 5.4).

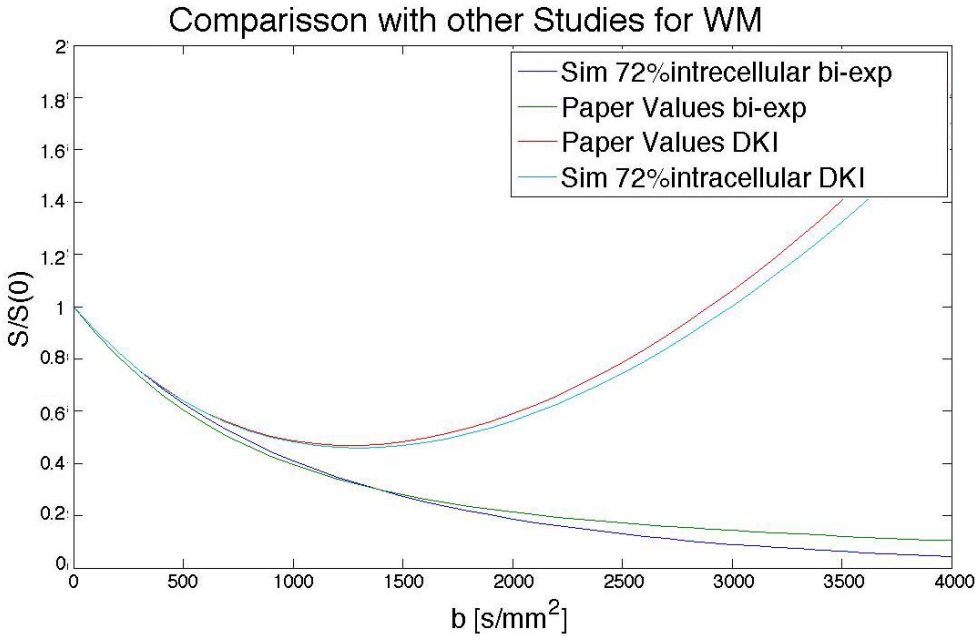

Figure 5.3: WM DKI and bi-exponential fit from measure data and simulation. Simulation data was the calculated from diffusion distribution.

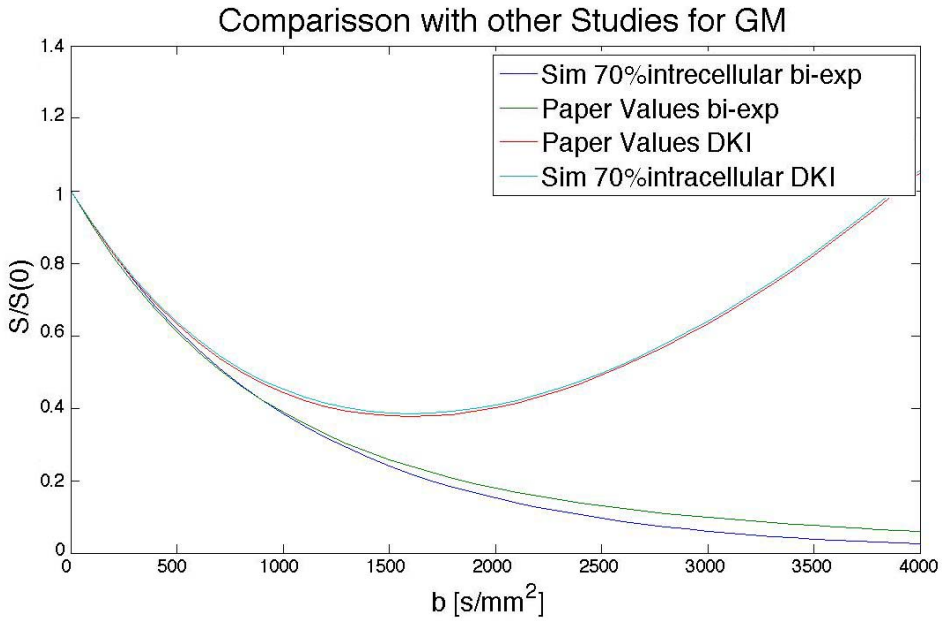

Figure 5.4: GM DKI and bi-exponential fit from measure data and simulation. Simulation data was the calculated from diffusion distribution.

A variation of the average cell diameters had nearly no impact on the ADC and AKC. This was to be expected as the diffusion time dependent changes had vanished within approximately 10 ms of diffusion.

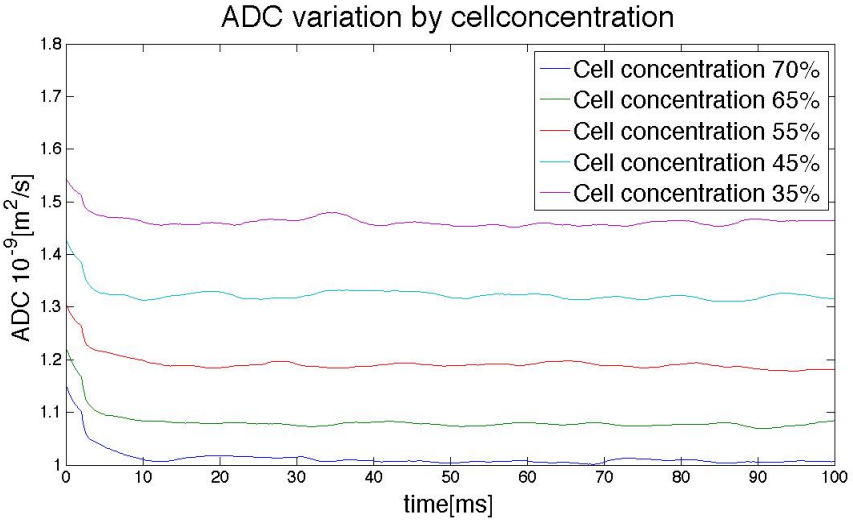

Figure 5.5: Variation of the ADC caused by variation of the cell concentration. The ADC is the mean diffusion coefficient of extracellular and intracellular volume.

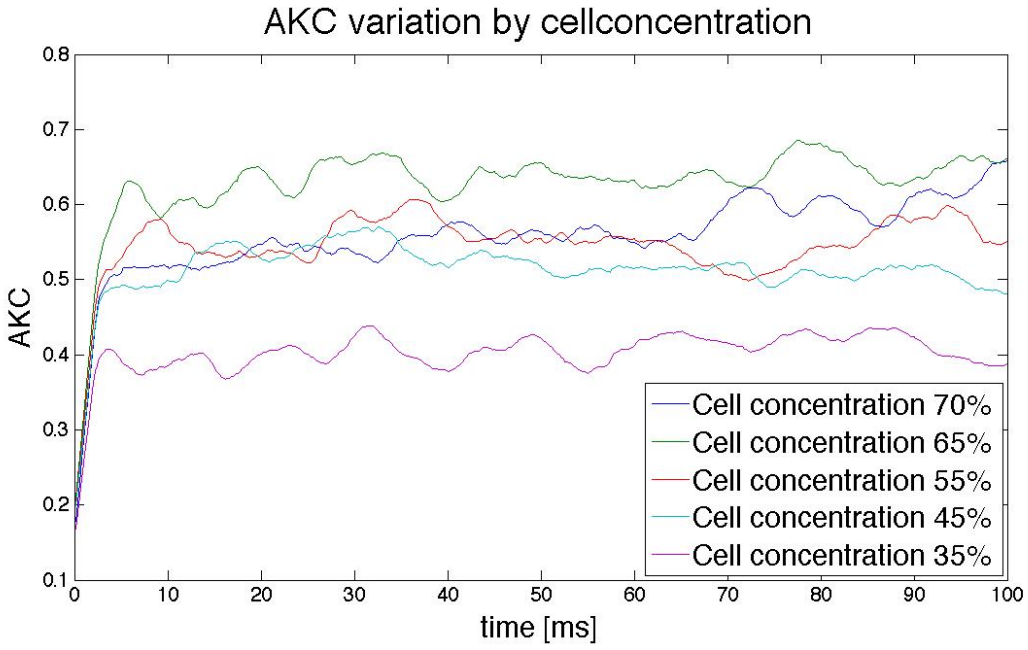

Figure 5.6: Variation of the AKC caused by variation of the cell concentration. It can be seen that the highest AKC is at a cell concentration of 65%. This is the case for the same diffusion speed in extracellular and intracellular space without substructure (with lower diffusion speed in the intracellular space the concentration will be higher).

Changing the cell concentration changed both ADC and AKC (Figure 5.5 and Figure 5.6). Therefore the ADC can be directly linked to the cell concentration (if the extracellular and intracellular substructur doesn't change). As the AKC also changes with the cell membrane permeability, the values had to be paired with the ADC at defined cell membrane behaviour. The membrane was chosen to be completely restricting for this purpose. This means that the highest possible AKC was paired with the ADC that is related to the cell concentration. If the measured AKC is lower than that, it has to be assumed that the diffusion through the cell membrane is increasing. Due to the fact, that the AKC is highest at the physiological state, estimating the effect of the cell membrane (and with that the demyelination) is less sensitive near physiological behaviour. Higher measured AKC can only be achieved, if the "free" diffusion coefficient in the intracellular space is lower than in the extracellular space. This is pretty likely the case, because of the DKI's methodical error.

Exchange of cells with fixed diameters to cells with highly varying cell diameters didn't have a significant effect on the ADC or AKC. No effect on the ADC was expected to show and for the AKC as well, as a permeable membrane would have been needed to separate the water pools for variation.

5.1.3 Simulation Validation

To validate the measure data, the model was slightly altered. The average axon diameter was kept but the single axons had random diameters to evaluate the impact of random diameters on the possible change of the ADC and AKC. Neither the ADC nor the AKC did change significantly with this altering. This wasn't clear, as the effect on the extracellular space could not be predicted.

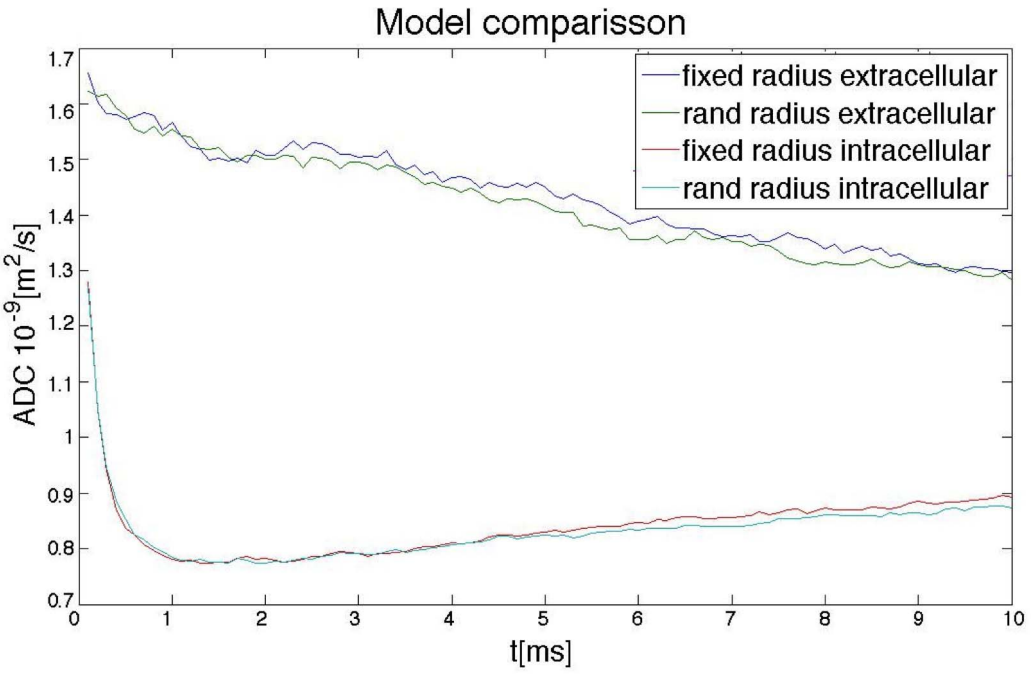

Figure 5.7: Variation of the ADC cause of random variation of the cell diameter for a structure with 65% cell concentration and a membrane permeability the lets 0.1% of the molecules pass.

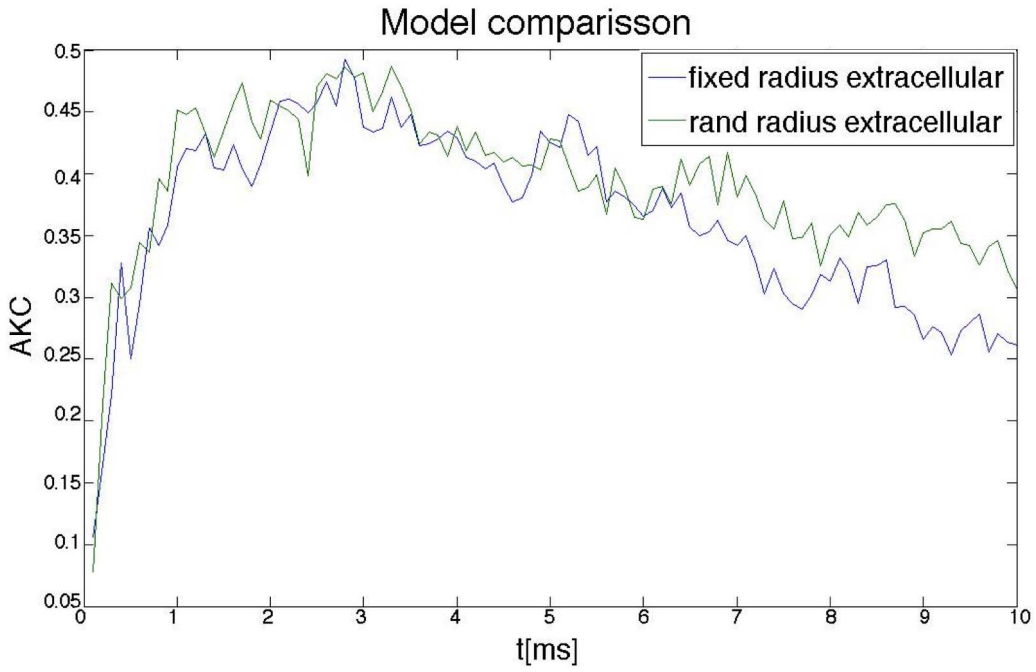

Figure 5.8: Variation of the AKC cause of random variation of the cell diameter for a structure with 65% cell concentration and a membrane permeability that lets 0.1% of the molecules pass.

5.1.4 Water Diffusion in the Intracellular Space

As the diffusion in the cell cluster has shown, different diffusion pools are only measurable, if there is an element that highly hinders or completely restricts diffusion. For this reason the diffusion within the cell can be analysed separately to get better information about the total water behaviour.

The intracellular space is a sponge like structure, which consists of cell organelles, and is surrounded by a diffusion hindering cell membrane. The structures in the intracellular volume and the cell membrane are surrounded by bound water, which has a faster signal intensity decay. Thus, the signal refers solely to the free moving water. The behaviour of the free moving cell water is a Brownian diffusion with a diffusion coefficient that can be calculated

as following: $0.44 \cdot D_{free}$ [38]. The diffusion coefficient of the intracellular volume was predicted to be about half the free water self-diffusion coefficient [23].

5.1.5 Single Cell Simulation

For the simulation the same model as for the cell cluster simulation was used with a diffusion restricting cell membrane and only one cell. All particles outside of the cell, where deleted to increase the calculation performance. This way the particles in the intracellular volume were in random positions, and the possibility for each position was the same. This is important for the estimation of the diffusion in the radial direction.

The diffusion coefficient was calculated using the free diffusion coefficient for water at $37°C$ $D_{free}(37°C) = 3.05 \cdot 10^{-9} m^2 s^{-1}$. This results in a diffusion speed of $1.34 \cdot 10^{-9} m^2 s^{-1}$ and consequently an average diffusion length in the radial direction of $7.3 \mu m$ in $10 ms$. With a cell radius set to $0.55 \mu m$ (physiological tissue is $0.4 \ldots 0.9 \mu m$ [34]) and $5 \mu m$ (to represent a pathological variation) the water movement in the radial direction was expected to be mainly affected by the cell diameter caused by the diffusion restriction of the cell membrane. The diffusion in axial direction was only modelled to see the effect of the diffusion restriction on the ADC and AKC. Which is not as easy to estimate, for the restriction in the radial direction clearly leads to a non-Brownian diffusion in this direction, which may effect the overall AKC. For this simulation about 100.000 particles were used and a step size of $10 \mu s$. The simulated data was sampled with every millisecond. This allows 100 steps between each sample. Therefore the resulting unrestricted diffusion can be assumed as Brownian motion. For the analysis the diffusion coefficient was measure in e_x and e_y which leads to the same results and therefore is equivalent to the diffusion in e_r as these vectors are in the same area.

As you can easily see (Table 5.1) the diffusion in the radial direction is already decreased after $1 ms$ and after $20 ms$ solely dependent on the diffusion restriction caused by the $10 \mu m$ cell diameter. This results in a constant term for the product of ADC and diffusion time. The time dependent change in a cell with diameter of only $1.1 \mu m$ is about three times as fast and the product of the diffusion time and the ADC is one third.

Diffusiontime Δ	$ADC \cdot e_x$	$ADC \cdot e_x \cdot 0.44^{-1} \cdot D_{free}^{-1}$	$ADC \cdot e_x \cdot \Delta$
$[ms]$	$[10^{-9} m^2 s^{-1}]$	$[\%]$	$[10^{-12} m^2]$
1	1.065	79	1.065
5	0.753	56	3.765
10	0.567	42	5.67
20	0.303	23	6.06
25	0.248	19	6.2
50	0.124	9.2	6.2
100	0.062	4.6	6.2

Table 5.1: Radial ADC variation in the intracellular space with diffusion time in an axon with $10 \mu m$ diameter.

This result can be used to calculate the ADC in the radial direction based on the radius of the axon. With equations (2.7) and (2.8) the variance of the Brownian motion is $24.8 \cdot 10^{-12} m^2$ which can be approximated by the second power of the axon radius (the error is about 1%). With this knowledge the diffusion in radial direction can be written as:

$$ADC_{radial} = \frac{r_{cell}^2}{4 \cdot \Delta} \tag{5.1}$$

if the diffusion time is long enough, which is approximately the case for:

$$\Delta \geq \frac{4 \cdot r_{cell}^2}{4 \cdot D} \tag{5.2}$$

The three-dimensional ADC and AKC can be seen in (Figure 5.9, Figure 5.10) and it's clear that even with a change in AKC in the radial direction, the overall AKC is still zero, which means that macroscopically, only in radial direction of intracellular water motion is different from Brownian diffusion but not the overall water motion. But this effect can only be seen by means of diffusion tensor imaging (DTI). The simulation was with only one cell, which means that the macroscopic AKC of a cluster is smaller than the AKCs of the single cells in it, because the diameters are Gaussian distributed. Therefore the distribution of the water in the radial direction will be multiplied with a Gaussian distribution, which will make the result

more Gaussian like. The ADC is affected by the diffusion restriction in the radial direction. The variance of cell diameter in a cluster has no effect on the ADC if the cell concentration and average diameter stays the same (as shown in the cluster studies) as the ADC is linked to the area in the radial direction, which doesn't change if the average diameter stays the same. Also small changes in average diameter have low impact on the ADC as the diffusion in radial direction is much smaller than the axial direction.

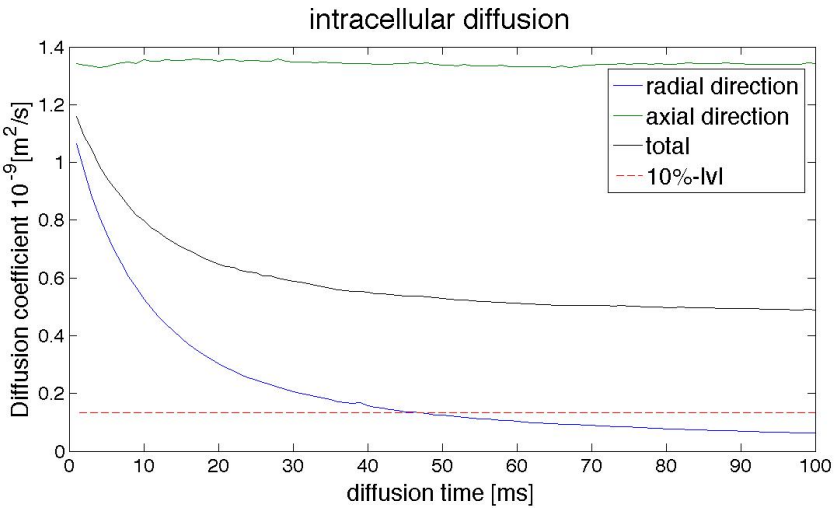

Figure 5.9: Variation of the ADC (total and in different directions) in the intracellular space.

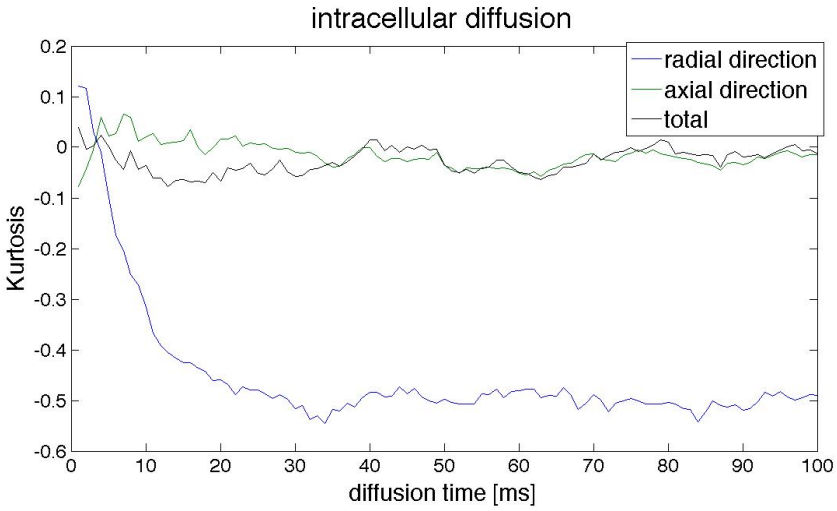

Figure 5.10: Variation of the AKC (total and in different directions) in the intracellular space.

5.1.6 Water Diffusion in the Extracellular Space

As in the intracellular space the behaviour of water in the extracellular space can be looked at separately. Because diffusion in the extracellular space is said to be only affected by toruosity, the values simulated for the extracellular volume can be used to simulate the effect of the substructures in the EMC on the diffusion in the extracellular space, which is not only affected by the cell membranes, but also by diffusion through the ECM and the water that's bound to that structure. As mentioned earlier the ECM can decrease to 4% of the total volume in case of ischemia. This leads to the assumption that the concentration of substructures in the extracellular volume is at best 20% of the extracellur space that covers only 20% of the total volume. As the tortuosity is independent from the diffusion coefficient, it was set to $D_{free} = 10^{-9} m^2 s^{-1}$.

5.1.7 Simulation of the Diffusion in the Extracellular Space

For this simulation the same model as for the diffusion in the cell cluster simulation was used, but the water molecules started randomly located at the boundaries of a circle around one cell. That was half the distance between the centre of two cells and the permeability of the cell membranes was zero, as it was in the single cell simulation. To compare certain results a second model was made that used a quadratic array with infinitely long rectangular prisms with square shaped cross-section areas instead of cylinders.
The reduced diffusion coefficient for the prism model can be estimated by:

$$D_x = D_y = \frac{1-a}{1-a^2} \cdot D_{free} \tag{5.3}$$

where a is the cell concentration. This shows, that the limes for $a \Rightarrow 1$ will be $D_x = D_y = 0.5 \cdot D_{free}$. Therefore the total diffusion coefficient with D_z being unaffected can decrease to $D = \frac{2}{3} \cdot D_{free}$. Using this estimation for a volume filled with cubes has the same diffusion coefficient at 100% cell concentration. On the other hand the diffusion in each direction turns out to be the same. By calculating the average diffusion coefficient for the

prism model, the cube model diffusion coefficient in each direction is also calculated at the same concentration.

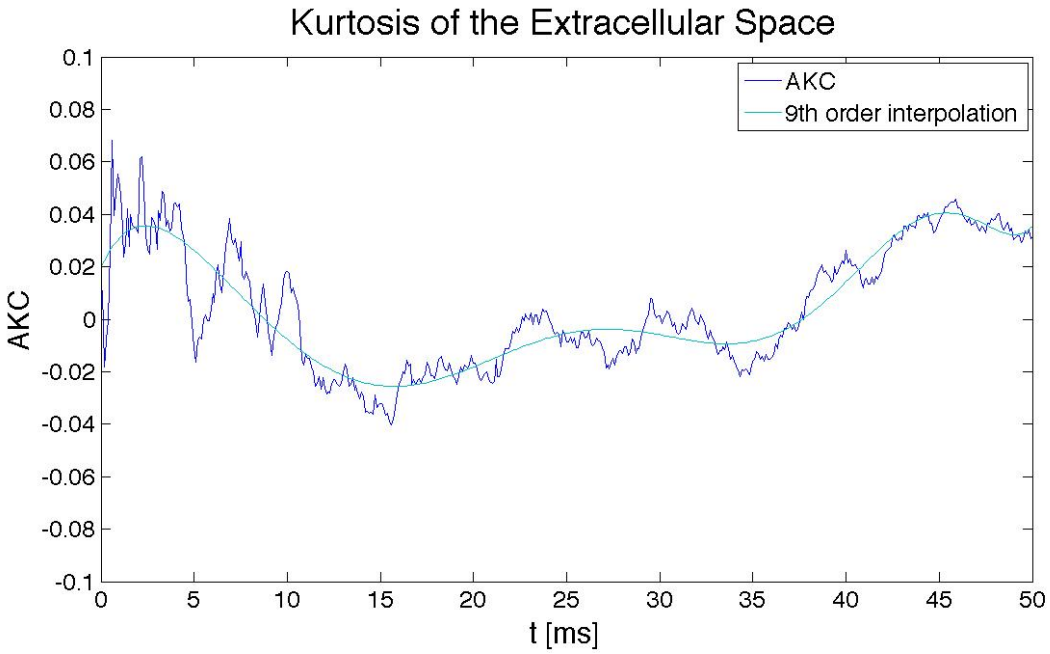

Figure 5.11: The AKC of the simulation data in the extracellular space in normal direction to the axons direction at 75% cell concentration. This value is below 0.1 which means it just consists of the simulation error.

As shown in Figure 5.11 the tortuosity caused by the cell membrane and substructures, does not lead to a measurable AKC. This was already expected, as a small water exchange through the cell membrane changes the AKC to zero. In case there is no structure separating the diffusion pools only an extremely high cell concentration (over 90% for cylinders or 99% for prisms) could have a similar effect. Note that the change in the diffusion speed decreases with cylinders below the lowest possible value for the prism structure and that the decreases of the ADC is more linear.

a	$ADC_{x,sq} \cdot D_{free}^{-1}$	$ADC_{sq} \cdot D_{free}^{-1}$	λ_{sq}	$ADC_{x,rad} \cdot D_{free}^{-1}$	$ADC_{rad} \cdot D_{free}^{-1}$	λ_{rad}
[%]						
10	0.90	0.93	1.04	0.92	0.95	1.03
20	0.82	0.88	1.07	0.85	0.90	1.05
30	0.74	0.83	1.10	0.80	0.87	1.07
40	0.69	0.79	1.13	0.75	0.83	1.10
50	0.64	0.76	1.15	0.72	0.81	1.11
60	0.60	0.73	1.17	0.67	0.78	1.13
70	0.57	0.71	1.19	0.61	0.74	1.16
75	-	-		0.57	0.71	1.19
80	0.54	0.69	1.20	0.54	0.69	1.20
85	-	-		0.47	0.65	1.24

Table 5.2: Radial ADC variation in the intracellular space with diffusion time in an axon.

5.2 Analysis of simulation results

5.2.1 Overall Water Diffusion

As shown above, the water pools have to be separated from each other. Else the exchange rate between the diffusion pools would be too fast as to measure two different diffusion pools. As a matter of fact, more than two diffusion pools are likely to appear in the cell cluster, but due to high exchange rates, it seems like only two diffusion pools. As for WM the exchange between intracellular and extracellular space is so small that it can be ignored. This enables to estimate the behaviour for each pool separately and to predict the overall water behaviour by the right combination of those two water fractions. The myelin water is the third existing pool, but because of fast spin-spin relaxation the signal intensity decays too fast to have any effect on diffusion weighted images. But it's still important for the calculation of the overall behaviour. As the cell concentration estimated by Charles Nicholson and Eva Sysková et al 1998 [32] includes the myelin water fraction, it has to be removed from the intracellular space.

5.2.2 Calculation of the Water Diffusion

5.2.3 Free Water Pools

It's likely that the free water pool in the intracellular and extracellular spaces is less than 100%. Therefore an educated guess for both pools is important. As we already know, the structure and bound water in the ECM is at best 20%. This leads to a signal of about 16% of the liquor at $b = 0$ from the extracellular area assuming also covers 20% of the total volume. Adding the myelin water fraction with additional 10%, the intracellular volume is left with 70% of the volume. The average signal from a healthy brain is between 25%…30% of the signal in the liquor, and the signal from the extracellular space is 9%…14% of the liquor signal. This means the free water concentration within the cell is 13%…20%.

5.2.4 Behaviour of Free Water Pools with Cell Concentration

The above calculated values fit pretty well for a healthy brain but terribly fail for pathological cases with low cell concentration. Because signal increases at $b = 0$ of up to 90% of the liquor signal are possible, which is more than the volume of the bulk water of the extracellular volume without cells in it (highest possible bulk water fraction). Therefore the concentration of free water in the extracellular volume has to increase with a decreasing cell concentration. This leads also to an increase of free water in the intracellular space.

For the change of free water pool concentration a linear fit was chosen. As two points for the concentration of substructures in the ECM are known (20% at 20% extracellular and 0% at 100% extracellular volume) the estimation is:

$$a_{free,ex} = 0.75 + 0.25 \cdot f_{ex} \tag{5.4}$$

with a linear link between intracellular space and extracellular space, the concentration in the intracellular space can be written as:

$$a_{free,in} = 1 - k + k \cdot f_{ex} \tag{5.5}$$

The simplest assumption of k being one, gives good fits for a low cell concentration but too low signals from the intracellular space at high cell concentrations. Therefore k was chosen to be slightly lower. Depending on the used noise model two different values for k give a good prediction of the actual signal. For the complex noise model a k of 0.9 and for the offset a k of 0.95 resulted in a good fit for both high and low cell concentrations. With these values the formulas are:

$$a_{free,in} = 0.1 + 0.9 \cdot f_{ex} \tag{5.6}$$

$$a_{free,in} = 0.05 + 0.95 \cdot f_{ex} \tag{5.7}$$

and with equation (2.25) and (5.4) we can write the normalised signal $S_0 \cdot S_{0,liquor}^{-1}$ at $b = 0$ as a function of f_{ex}.

$$\frac{S_0}{S_{0,liquor}} = \left(0.75 + 0.25 \cdot f_{ex}\right) \cdot f_{ex} + \left(0.1 + 0.9 \cdot f_{ex}\right) \cdot \left(1 - f_{ex}\right) \cdot 0.875 \tag{5.8}$$

$$\frac{S_0}{S_{0,liquor}} = \left(0.75 + 0.25 \cdot f_{ex}\right) \cdot f_{ex} + \left(0.05 + 0.95 \cdot f_{ex}\right) \cdot \left(1 - f_{ex}\right) \cdot 0.875 \tag{5.9}$$

where 0.875 is the ratio between the intracellular volume and the intracellular volume plus the myelin fraction (with 10% myelin fraction at 20% extracellular space). As the ratio of the signal and the liquor signal is known the size of the extracellular fraction can to be calculated.

$$f_{ex} = 1.349 - \sqrt{1.349^2 + 0.1628 - \frac{S_0}{0.5375 \cdot S_{0,liquor}}} \tag{5.10}$$

$$f_{ex} = 1.323 - \sqrt{(1.323)^2 + 0.075 - \frac{S_0}{0.581 \cdot S_{0,liquor}}} \tag{5.11}$$

The quadratic equation has two solutions but only the smaller solution makes sense, because the water fraction can't be higher than 100%.

For the substructure the intracellular space was assumed to be isotropic with a diffusion coefficient $D_{ax,in} = 0.44 \cdot D_{free}$ at 20% extracellular volume. The ECM was assumed to be mainly in the radial plane (fixations between axons), which has only little effect on the difference of the diffusion coefficients of this model compared to the isotropic behaviour (e.g. The diffusion coefficient difference for the extracellular space, caused by these two ECM-structures, is only 3% if the extracellular space covers 14.2% of the total volume. For

lower cell concentrations the difference is even lower.). The resulting formulas for the diffusion coefficients of the intracellular and extracellular water pools are:

$$D_{ex} = \frac{ADC_{x,rad}\left(a_{free,ex}\right) + \left(1 + ADC_{x,rad}\left(a_{free,ex}\right)\right) \cdot ADC_{x,rad}\left(f_{ex}\right)}{3} \tag{5.12}$$

$$D_{ax,in} = \frac{0.44}{0.69} \cdot ADC_{rad}\left(a_{free,in}\right) \tag{5.13}$$

$$D_{in,50ms} = \frac{D_{ax,in} + 0.081 \cdot D_{free}}{3} \tag{5.14}$$

The intracellular diffusion coefficient with a diffusion time of $50ms$ $D_{in,50ms}$, is a good estimation for the actual diffusion coefficient. A change of the cell diameter by the factor of two or the diffusion time by the factor 4 will lead to an approximation error of less than $\pm 10\%$.

$S_0 \cdot S_{0,liquor}^{-1}$	[%]	25	26	27	28	29	30	31	32	33	34	35
f_{ex}	[%]	14.2	14.9	15.7	16.4	17.1	17.9	18.6	19.4	20.2	20.9	21.7
$a_{free,ex}$	[%]	78.6	78.7	78.9	79.1	79.3	79.5	79.7	79.9	80.0	80.2	80.4
$S_{ex} \cdot S_{0,liquor}^{-1}$	[%]	11.1	11.8	12.4	13.0	13.6	14.2	14.9	15.5	16.1	16.8	17.5
$D_{ex} \cdot D_{free}^{-1}$	[%]	56.3	56.9	57.6	58.3	59.0	59.7	60.3	61.1	61.7	62.0	62.4
f_{in}	[%]	75.1	74.5	73.8	73.2	72.5	71.9	71.2	70.5	69.9	69.2	68.5
$a_{free,in}$	[%]	18.5	19.2	19.9	20.6	21.3	22.0	22.7	23.4	24.2	24.9	25.6
$S_{in} \cdot S_{0,liquor}^{-1}$	[%]	13.9	14.3	14.7	15.1	15.4	15.8	16.2	16.5	16.9	17.2	17.6
$D_{ax,in} \cdot D_{free}^{-1}$	[%]	43.3	43.6	44.0	44.1	44.4	44.5	44.7	44.9	45.1	45.2	45.5
$D_{in,50ms} \cdot D_{free}^{-1}$	[%]	17.1	17.2	17.4	17.4	17.5	17.5	17.6	17.7	17.7	17.8	17.9
$ADC_{true} \cdot D_{free}^{-1}$	[%]	34.5	35.1	35.8	36.3	37.0	37.5	38.1	38.7	39.2	39.6	40.1
AKC_{true}		0.96	0.95	0.95	0.95	0.95	0.95	0.94	0.94	0.94	0.93	0.92

Table 5.3: Calculated diffusion behaviour for physiological tissue without considering cell membrane permeability.

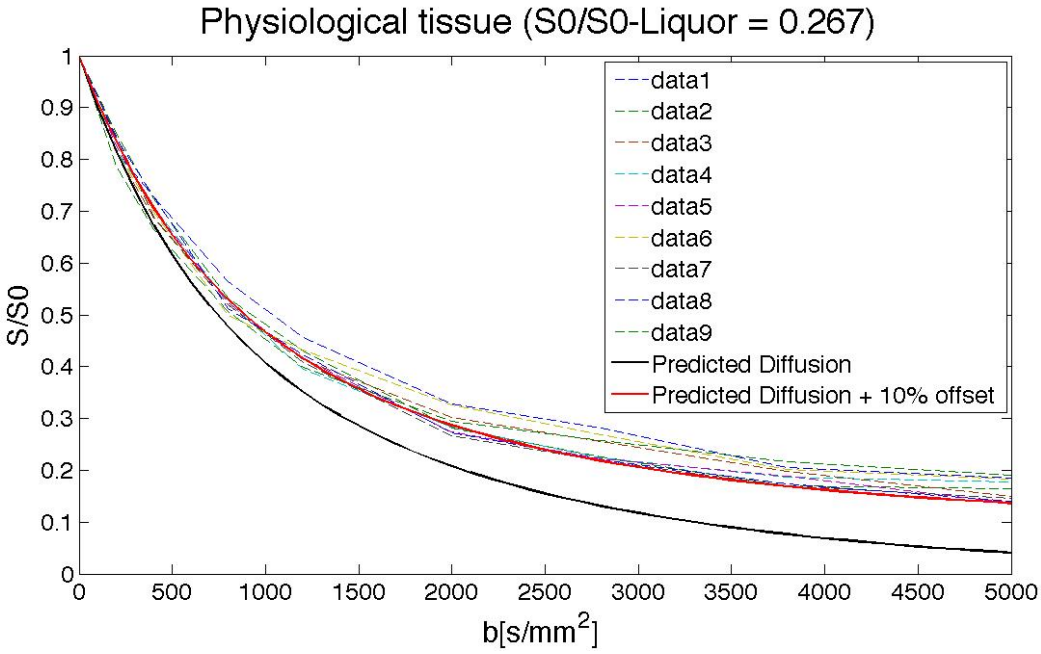

Figure 5.12: This figure shows the behaviour of water diffusion due to diffusion restricting and hindering effects estimated by the calculation based on the simulation compared to the measured data. The offset might be either caused by noise or by a third water pool that has nearly no diffusion. The cell membrane permeability seems to be ignorable but the offset has some variation.

$S_0 \cdot S_{0,liquor}^{-1}$	[%]	60	63	66	69	72	75	78	81	84	87	90
f_{ex}	[%]	43.3	46.2	49.3	52.4	55.7	59.2	62.8	66.6	70.7	75.0	79.7
$a_{free,ex}$	[%]	85.8	86.6	87.3	88.1	88.9	89.8	90.7	91.7	92.7	93.8	94.9
$S_{ex} \cdot S_{0,liquor}^{-1}$	[%]	37.1	40.0	43.0	46.2	49.6	53.2	57.0	61.1	65.5	70.4	75.7
$D_{ex} \cdot D_{free}^{-1}$	[%]	72.4	74.2	75.4	76.4	77.4	78.4	80.8	81.6	83.4	85.3	87.4
f_{in}	[%]	49.6	47.1	44.4	41.6	38.7	35.7	32.5	29.2	25.6	21.8	17.7
$a_{free,in}$	[%]	46.1	48.9	51.8	54.8	58.0	61.2	64.7	68.3	72.2	76.3	80.8
$S_{in} \cdot S_{0,liquor}^{-1}$	[%]	22.9	23.0	23.0	22.8	22.4	21.9	21.0	19.9	18.5	16.7	14.3
$D_{ax,in} \cdot D_{free}^{-1}$	[%]	50.9	51.4	51.9	52.3	52.7	53.2	54.1	55.0	55.9	56.7	57.6
$D_{in,ax} \cdot D_{free}^{-1}$	[%]	19.7	19.8	20.0	20.1	20.3	20.4	20.7	21.0	21.3	21.6	21.9
$ADC_{true} \cdot D_{free}^{-1}$	[%]	52.3	54.3	56.1	57.8	59.7	61.5	64.6	66.7	69.7	73.1	77.0
AKC_{true}		0.72	0.70	0.66	0.63	0.59	0.55	0.51	0.46	0.41	0.35	0.29

Table 5.4: Calculated diffusion behaviour for pathological tissue, that has been altered by past TIAs, without cell membrane permeability.

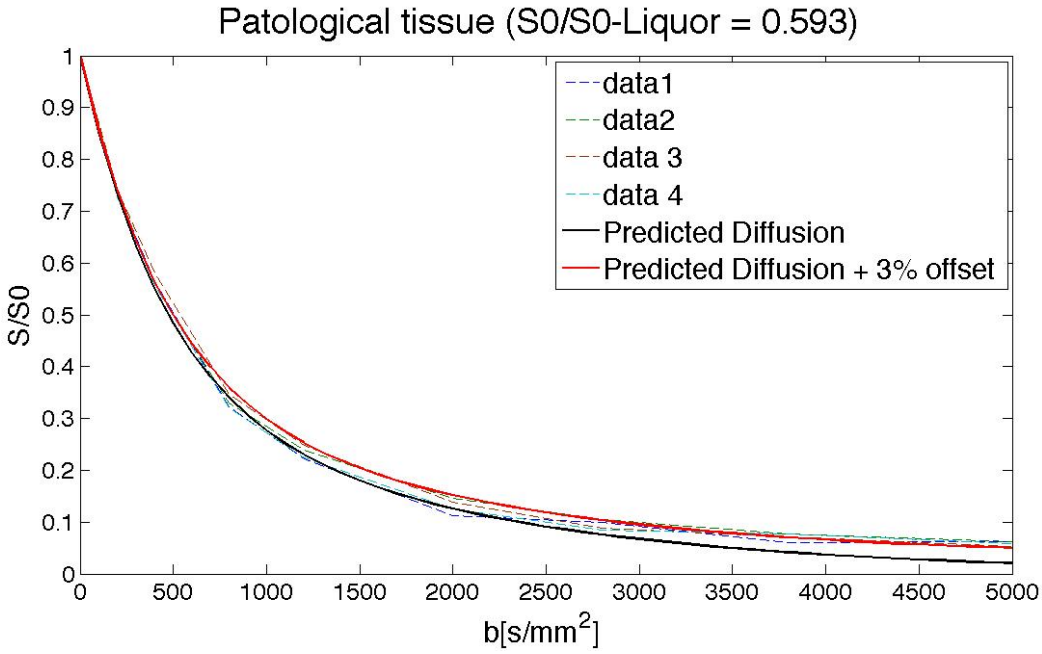

Figure 5.13: This is the comparison of tissue that was changed by previous TIAs with the calculated data from the simulation. Both, the relative and absolute offset, is lower compared to physiological tissue. This leads to the assumption that if a third water pool causes it, the cells responsible for it are fewer too. The faster signal decay at low diffusion weighting might be caused by high cell membrane permeability.

5.3 Interpretation of Measured Data

5.3.1 Noise

The standard distribution of the fitted parameters for DKI with a SNR of only five is with less than 10% for the ADC and 20% for the AKC much more robust than the bi-exponential fit. This was the result for the predicted diffusion behaviour of an area with the signal to liquor signal ratio of 26.7% (without diffusion weighting) and 50 averages. In comparison the bi-exponential fit showed a standard derivation of 50% for the fast diffusion coefficient and 120% for the slow diffusion coefficient. Moreover the adding of the noise to the simulation data has shown, that for high *b*-values the measured signal is mainly caused by signal noise.

So high diffusion weighting doesn't lead to additional information about the underlying tissue. Instead noise mainly effects the fitted parameter. This is especially important, as bi-exponential fits need higher diffusion weighting for a good fit of the slow diffusion pool parameters. Both fits have a significant parameter change caused by noise. But the low standard derivation of the fitted DKI parameters, have a significant advantage. The noise free parameters can be estimated if the standard derivation of the noise is known. This gives the possibility to achieve knowledge of the underlying tissue and compare data derived from different measurements.
Both parameters have a significant parameter change caused by noise compared to noiseless data. But within a small noise variation DKI has a lower standard distribution than bi-exponential fits. Thus the actual noise free parameters for DKI can be estimated if the standard derivation of the noise is known and from it, using the simulation data knowledge of the underlying tissue can be achieved.
The use of two different noise models has shown, that an offset added to the simulation data leads to a better fitted curve than the complex noise model. This can either be related to the permeability of the cell membrane or an additional water pool (with no measurable ADC).

5.3.2 Complex Noise

The complex noise has nearly no effect on the ADC but leads to an increase of the fitted AKC of up to 40% compared to the fitted noise free simulated data with a fit using for both of $b = 0 \ldots 2 \cdot 10^9 s \cdot m^{-2}$ and SNR of five. The same difference occurs for $b = 0 \ldots 3 \cdot 10^9 s \cdot m^{-2}$. But the variation of the fit is robust. If the SNR (without averaging) is above ten at $b = 0$ the change of the AKC is minimal.

5.3.3 Offset

The offset model results in a lower increase of AKC but also results in a small increase of ADC. This noise model also leads to a higher standard derivation for both AKC and ADC. The offset model used on the simulation data leads to a curve that better fits the measured data than the complex noise model. This can be explained in two ways. The first explanation is that the noise is actually complex and the permeability of the cell membrane leads to an exchange between the water pools. This results in less signal intensity loss at b-values of $1\ldots2\cdot10^{9} s\cdot m^{-2}$. The permeability of the cell membrane can't explain why the signal in WM is higher than expected for high b-values (this would mean that in WM noise is increased). The other explanation is, that there is a third water pool (consisting of less than 25% of the total free water fractions). This water pool has no apparent diffusion. This can be caused by a spherical shaped cell membrane with a rather small diameter of a maximum of $2.5\mu m$. As the soma exists in both WM and GM and the diameter has to be at least $50\mu m$ for a significant signal change, the pool has to be located in other cells than the neurons. Some proposed that part of the bound water fraction has no exchange with the free water pool. This was explained by slow water diffusion in the bound water. But the higher WM signal at high b-values compared to GM cannot be explained.
As long as the origin of the water pool without apparent diffusion is not clearly understood, the signal can be assumed as a noise offset for the estimation of the parameters of the remaining two water pools. It's also possible that this third water pool (that seems to mainly exist in WM an therefore might be related to myelination) caused the AKC change between WM and GM and that the permeability for the cell membrane in both cases is the same.

5.3.4 Measured Data and the Third Water Pool

The signal intensity for higher diffusion weighting should always be the same or lower than for lower diffusion weighting. This is the case for b-values below $2\cdot10^{9} s\cdot m^{-2}$. If these values are higher, noise can cause different changes if the signal intensity change caused by

diffusion is smaller than the noise. But the different signal offset is probably related to a third water pool. This can only be the case if diffusion restrictions limit the water movement. In table (Table 5.5) you can see a few measured points where the signal increased at higher *b*-values. This happens seldom, as normally a small signal loss is still present, but the signal often hardly changes at the high diffusion weightings.

	$S(0)$	$S(2.8\cdot 10^9 s\cdot m^{-2})$	$S(3.8\cdot 10^9 s\cdot m^{-2})$	$S(5\cdot 10^9 s\cdot m^{-2})$
Patient 2 (79/71)	172	44	27	31
Patient 3 (52/62)	216	65	45	50
Patient 3 (79/72)	225	49	40	46
Patient 4 (53/59)	231	54	41	45
Patient 4 (79/73)	249	42	47	40
Patient 4 (53/59)	238	38	43	35

Table 5.5: Patients with high changed areas in the brain, seem to have other areas with high signal intensities at high diffusion weighting and low signal decrease.

5.3.5 Optimal *b*-Factors

The noise study shows that a few *b*-values from zero up to $2\cdot 10^9 s\cdot m^{-2}$ are needed. Higher *b*-values do not increase the stability of the fit and are therefore not necessary. The comparison of the actual and fitted AKC based on the simulated data shows an already significant AKC decrease at $b = 2\cdot 10^9 s\cdot m^{-2}$ (30% in case of healthy tissue).

5.3.6 Ischemia

In ischemia, the cells swell and decrease the extracellular space significantly. As this process is rather fast, structural changes will come later (when the T_2-weighted image changes). Because of this we can assume that the free water fraction in the intracellular space increases and decreases in the extracellular space, but both free water fractions together will still have

the same part of the volume as they had before the swelling. The extracellular space can become as small as 4% of the total volume. This largely decreases the water diffusion in the extracellular space and increases the signal given by the intracellular volume. Thus the ADC decreases significantly below the predicted value at the given signal to liquor signal ratio. For an estimation of a maximum possible ADC in ischemic tissue, the ADC was be calculated at 10% cell concentration. The slower ADC in the extracellular space due to the lower free water fraction was taken into account. The change in diffusion caused by a higher cell concentration was not considered in this calculation, because it's not possible to simulate tissue with only 10% extracellular space in an adequate time with my model, as the lowest extracellular space would be 9.5% which means that the distance between the cells is so small, that the step size for random walk model would be a few ns. This would also require another self-diffusion equation, as the modelled water diffusion with Einstein coefficients doesn't take into account the case of only a few collisions between the water molecules. The associated Langevin equation would have to be used to simulate the correct behaviour of water within one time step (else the effect of the cell membrane for the shortest distance might not be simulated correctly).

The shift of free water from the extracellular space into the cells, from 14.2% to 10% extracellular volume decreases the ADC from $1.05 \cdot 10^{-9} m^2 s^{-1}$ to $.75 \cdot 10^{-9} m^2 s^{-1}$ and the AKC from 0.96 to 0.63 (though the AKC might vary due to noise, cell membrane permeability and methodical error). The appearing shift from the fast to the slow diffusion pool lowers the ADC since it is the weighted average of the diffusion coefficient of the free moving water pools. In previous studies ADC decreases of 30% to 50% were measured during ischemia [46,29]. This is can be seen in this simulation too, as the ADC decreases by about 25% for a case of small water shift due to the intracellular space. This means the ADC change can be fully explained by shift of water.

5.3.7 Demyelination of Tissue

Demyelination results in a higher permeability of the membrane-myelin complex that hinders diffusion between extracellular and intracellular space. As it can be seen in GM, the ADC remains constant if the permeability doesn't get too high, but the AKC is sensitive to change in permeability. An interesting fact is, that the AKC is not significantly different from zero before permeability changes have an effect on the ADC. Accordingly the ADC is a measuring tool for the ratio between extracellular and intracellular fractions and the AKC turns out to be a parameter to estimate the myelination, which changes with both the cell concentration and the permeability of the cell membrane (including the diffusion hindering effect of the myelin sheath). It's important to state, that noise has an impact on both values and too high b-weighting also lowers the AKC. Although comparing AKC of different b-values shows this effect, it doesn't mean that in the case of the lower AKC the demyelination has taken place.

6 Discussion

6.1 Diffusional Kurtosis Imaging and Image Noise

The SNR before averaging has a significant impact on the fitted AKC but nearly no impact on the ADC, which makes estimations using the ADC pretty accurate. In case of the AKC, the parameter changes significantly with change of the SNR, but it has a much smaller standard derivation than the parameters of the bi-exponential fit as long as the highest b-value is at least $2 \cdot 10^9 s \cdot m^{-2}$. Increasing the diffusion weighting even higher results in the AKC being mainly affected by noise and the methodical error caused by the second order Taylor series. This can be easily seen by use of b-values above $3 \cdot 10^9 s \cdot m^{-2}$, where noise has an increased relative and sometimes even absolute error, while the parameter value decreases. Therefore the optimal b-weighting is a series of diffusion weightings up to $b = 2 \cdot 10^9 s \cdot m^{-2}$. The slightly higher standard derivation in the measured data sets might be due to the smaller amount of data that was used for the parameter fit.

Based on the fact, that the apparent kurtosis coefficient is significantly dependent on the SNR before averaging but doesn't change much if the SNR stays the same, measuring the actual signal to noise ratio becomes a promising enterprise. The kurtosis depends on the relation between the diffusion coefficients and their fraction ratio. As noise at high b-weighted signals can have significant impacts on the averaged signal (equation (2.48)) the ratio between a fast and a slow diffusion coefficient seems to increase. It can be seen in an increase of the AKC caused by low SNR. This makes one single high b-weighted image

important for the estimation of the SNR to give better predictions using DKI. It includes a probable existence of free water pools with no apparent diffusion coefficient. As the signal won't be lowered for high b-weightings the signal is altered by these pools and as long as the origin is not clearly understood, the signal alteration is noise like for fit of the other water pool parameters.
Keeping the SNR before averages above ten results in low to even no impact of the SNR on the AKC. Note that the signal for healthy tissue is already lowered by spin-spin relaxation.

Increasing the order of the Taylor Series increases the accuracy of the fitted AKC at a loss of precision. Increasing the b-values for better precision will again lead to worse accuracy. Therefore a data array with fitted AKC vectors for different SNR, free water concentration and ADCs will lead to better results than increasing the order. The resulting AKC vectors would have information about the impact of cell membrane permeability on the measured diffusion. AKC value variations due to SNR variation and methodical error can be mapped to the true AKC which than can be compared between different measurements.

6.2 Cell Membrane and Diffusion Hindering Effects

Assuming the cell membrane is responsible, the simulation shows, that already a low exchange rate through the cell membrane has a significant effect on the AKC but not on the ADC. Thus, this result can be used to predict the behaviour of the effects of bound and free water pools on the diffusion coefficient. As the exchange between bound and free water is assumed to be higher than the exchange between extracellular and intracellular space, where water would have to interact with both cell membrane and bound water, the cell membrane plays an important role for the measuring diffusion effect, thought it is not the only reason as shown by Ackerman and Neil [38], who measured the diffusion coefficient of water in the intracellular space of Xenopus oocytes. The oocytes had a diameter of $10^{-3} m$, where the measured diffusion coefficient of water was 44% of the free diffusion coefficient and the motion appeared Brownian. This supports the assumption, that the exchange rate between

diffusion pools without a highly hindering barrier, like the cell membrane just results in an averaged ADC and not in two or more diffusion pools with different ADCs. The reduced diffusion in cells can be either interpreted by the fact, that bound water and cell structures hinder the diffusion or, that water switches between both pools and therefore the diffusion is reduced. As the exchange rate between the water pools is high enough, the effect on the measured signal is basically the same. Therefore the T_2-decay of bound water is not measure able without sequences that are so fast that nearly no exchange between bound and free water appears. As mentioned before some researches leaded to multi-exponential signal intensity decays in the intracellular space. This might occur due to the fact that intracellular space from other cells than neurones might also give significant signals (that might be a third water pool). The different structure might lead to diffusion restriction in three instead of two dimensions and therefore result in a third diffusion coefficient (one extracellular and two intracellular diffusion pools).

As the curve of predicted diffusion with added complex noise has a higher AKC than the measured data, it is most likely that the diffusion through the cell membrane is not completely restricted. This also explains why the AKC in GM is lower than in WM which has less myelinated areas and therefore a faster diffusion through the cell membrane. The diffusion through the cell membrane can be easily understood by the findings of water channels [3]. Though, as mentioned before, the diffusion through the cell membrane is still extremely hindered. On the basis of these facts demyelination can be measured by means of dropping AKC below values related to the measured signal loss from spin-spin relaxation and ADC. To be able to interpret the measured data correctly, noisy data has to be preprocessed. This is because the fitted AKC can be significantly increased by noise. Due to this effect a decreasing AKC which is related to an increase of the permeability of the cell membrane might not be recognized. As a matter of fact the noise doesn't have to be completely neutralized as a SNR above 10 (before averaging) shows a minimal change in the AKC. Note that the AKC significantly decreases with increased b-weighting. If the highest b-value is $2 \cdot 10^9 s \cdot m^{-2}$, the methodical error is 30% (for physiological tissue without noise). Therefore the diffusion weighting and SNR is important in case of data comparison.

6.3 Diffusion Decrease in Physiological Tissue Caused by Ischemia

As the data from my simulation has shown ischemia can cause ADC decreases between 25% and 50% (for ischemia in still undamaged tissue). In previous studies ADC decreases of 30% to 50% were measured during ischemia [46,29]. Therefore the ADC change can be fully explained by the shift of water. This contradicts the previous studies, which said that the shift of water from the extracellular space to the intracellular space has not enough effect to cause the diffusion decrease in ischemia. The calculation for the diffusion for the diffusion speed in ischemic tissue didn't take into account that the diffusion in the extracellular space also decreases. This means the lowest diffusion decrease caused by ischemia is slightly higher than calculated. For the highest estimated diffusion decrease, it has to be noted, that a movement of the complete free water pool from the extracellular volume to the intracellular volume is rather unlikely and therefore the estimated diffusion decrease will probably not occur in measurements (40% decrease is normally named for diffusion decrease). Taking into account that the diffusion can decrease more than actually measured, it is proven that water shift can cause the diffusion decrease.

6.4 Diffusional Kurtosis Imaging and Spin-Spin Relaxation

The ADC is related to the cell concentration and the free water concentration in both the extracellular and intracellular water pools. Therefore, if the signal increases due to slower spin-spin relaxation, the ADC increases as the free water pools increase. The increase of the water is related with a decrease of cell concentration and therefore the free water fraction in the extracellular space increases faster than in the intracellular space. On the other hand if the ADC drops without changes in spin-spin relaxation, the reason is most likely cell swelling without change in substructures. As a consequence, the apparent diffusion coefficient drops, as the coefficient for both intracellular and extracellular space hardly changes at all. But the

free water fraction moves from extracellular space to the intracellular volume. As the movement within the cell is much slower due to diffusion hindering effects the measured diffusion coefficient decreases. The more water moves from one pool to the other, the larger is the drop (If only the ECM remains outside the cell, the diffusion coefficient drops as low as the diffusion in the intracellular space which is about as low as 15% of the free self-diffusion coefficient of water at 37ºC.). Taking into account that the diffusion in the intracellular space may increase due to the higher concentration of free water, the diffusion still decreases significantly (about 16.6% for tissue that wasn't damaged before the cell swelling). Thus, ischemia leads to a much lower ADC than expected. If the ADC is compared with the T_2-weighted signal ratio of the tissue and the liquor, the ADC drop can even be seen, when the ADC is still higher than in physiological tissue (due to past damage in the brain for example from former TIA). It has to be pointed out, that the diffusion decreasing effect in that case might not be as high as in healthy tissue, as the intracellular space is much smaller.

This means the information from T_2-weighted images has information about the sum of both free water fractions. This explains the fact, that shortly after the approach of an ischemia the spin-spin relaxation doesn't change significantly. It happens after the pathology has caused permanent changes to the underlying tissue. As long as just the water fraction moves, only the ADC changes. This means that appearing hyperintense areas in T_2-weighted images represent areas with tissue abnormalities. Based on this it was assumed that these hyperintense areas are in locations that have been severely damaged which finally resulted in cell death. But simultaneously the axon myelination was assumed to be intact. Thus the extracellular space increased compared to physiological tissue and with that the ADC increased and both the AKC and the spin-spin relaxation decreased. The unchanged myelination excludes an AKC change caused by the change of permeability.

The change in the AKC has two different reasons. First the increased signal from slower spin-spin relaxation increases the SNR significantly which decreases the AKC and secondly the fact, that the ratio between free intracellular water and free extracellular water decreases. The highest AKC without changing ratio of ADCs from extracellular space and intracellular space is when the intracellular free water has about 65% of the total free water (if the "free" diffusion coefficient is the same in both pools).

7 Conclusion

The diffusional kurtosis approach has robust parameter fit with an ADC that can be directly linked to the weighted average of the apparent diffusion coefficients of the existing bulk water pools. As ischemia can cause shifts between the free water diffusion pools, the ADC can change significantly without a significant change of the T_2-weighted image. This represents a transient change of the underlying tissue. Permanent change of the underlying tissue results in a change of the ADC and T_2-weighted image. If the ADC is paired with the spin-spin relaxation, transient water shifts can even be monitored in permanently changed tissue. The AKC needs preprocessed measured data. This is because the AKC is sensitive to a lot of different effects (noise, diffusion coefficients, cell membrane permeability, diffusion weighting). For preprocessing the signal offset, caused by noise and a probably third bulk water pool, has to be compensated. Only than the permeability of the cell membrane can be put directly into relation with the AKC. As the AKC also changes with change of the cell concentration and b-weighting, it has to be paired with the ADC for possible predictions.
The relation between the increased signals in white matter compared to other tissues should be further investigated to get more information about the underlying tissue.

Appendix A

Simulation Code

```
%% Diffusion in White Matter
%   This version is to simulate the behavier
%   of water molecule in white matter. As far
%   as it's implemented here it only simulates
%   the movement of water in and around 1 cell.

%   to do list:
%   *calculate for more cells. (80e-6m*80e-6m array)
%   *calculate total way of each molecule
%   *fit the curve using:
%       +diffusional kurtosis fit
%       +biexponential fit

%   Diplom. Theses
%   Diffusional Kurtosis Imaging
%   Nausner Christoph
%   July 2009

%% general initialization
% clear
resume = 0;
figure(1); clf;
set(gcf,'doublebuffer','on');  % for smooth animation
%alpha = 10^-3; % chance to penetrate the membrane
alpha = 0;
% (alpha = 0 ... means restricted diffusion)
% (alpha = 1 ... means unhindered diffusion)
%Dh2o = 2.1; % Free diffusion of water at 20 C 10^-9[m^2/s]
%Dh2o = 2.272; % Free diffusion of water at 25 C 10^-9[m^2/s]
Dh2o = 3.05*.44; % Free diffusion of water at 30 C 10^-9[m^2/s]
deltaT.t = 0.05; % steplengh in [ms]
%deltaT.t = 0.001; % steplengh in [ms]
deltaT.tred = 1; % reduced time resolution [ms] ... should be at least 20 times bigger than steplengh
deltaS.mean = (6*(Dh2o)*deltaT.t)^.5; % steplength [1e-6m]
deltaT.tred_fac = deltaT.tred/deltaT.t;
gainex = sqrt(1);

%% Simulation area and number of Zells
simTime = 100; % Simulation Time [ms]
%boundary.density = 0.795;
boundary.density = 0.6;
boundary.number = 23;
```

```
boundary.radius = 5*ones(boundary.number, 1);
%boundary.radius = 2.2*ones(boundary.number, 1);
boundary.distance = max(boundary.radius).*(pi()/boundary.density*2/(3^.5))^.5; %boundery density calculation for hexagonal structur
% Random cell radius
%boundary.radius = 0.45 + 0.2*rand(boundary.number, 1);
%boundary.radius = boundary.radius.*(0.55^2/mean(boundary.radius.^2)).^.5; %correctur for rand cell radius so % intra/extra cellular
volumina stays the same.
simLimit.x = 2*boundary.distance; % Simulation area in x direction [?m]
simLimit.y = sqrt(3)*boundary.distance; % Simulation area in y direction [?m]

%for rand rad
%varR = (0.55+.055*rand(11,1));
%varR = sqrt(((varR.^2)./mean(varR.^2)).*.55^2);
%boundary.radius(6:9) = varR(1:4);
%boundary.radius(11:13) = varR(5:7);
%boundary.radius(15:18) = varR(8:11);

%% create particles and specify intial position

if resume == 0
   particle.nTotal = 50000;                          %number of simulated water molecules
   startregion.x = boundary.distance;
   startregion.y = sqrt(3)/2*boundary.distance;
   particle.xStart = rand(particle.nTotal, 1).*(2*startregion.x)-startregion.x;  %initial position in x direction
   particle.yStart = rand(particle.nTotal, 1).*(2*startregion.y)-startregion.y;  %initial position in y direction
%     particle.Phi = rand(particle.nTotal, 1)*2*pi;
%     particle.xStart = 1/2*boundary.distance.*cos(particle.Phi);
%     particle.yStart = 1/2*boundary.distance.*sin(particle.Phi);
   particle.zStart = zeros(particle.nTotal, 1);
   particle.xPos = particle.xStart;
   particle.yPos = particle.yStart;
   particle.zPos = particle.zStart;
   particle.xResume = particle.xPos;
   particle.yResume = particle.yPos;
   particle.zResume = particle.zPos;
else
   particle.xPos = particle.xResume;
   particle.yPos = particle.yResume;
   particle.zPos = particle.zResume;
end

%% plot particle locations and save plot handle

hplot = plot(particle.xPos, particle.yPos, 'b.');
hold on;

% adjust axis properties
% as the simulation is 2D in case of bounderies, there is no ax limit for z
% direction. The limits for x and y are choosen to use elastic reflection
% at the bounderies to simulate a molekule that came from ouside the
% bounderies by creating a mirror image of the starting position outside
% the simulated area.
axis equal         % ensure equal xy scaling
axLimit.x = simLimit.x+boundary.distance;
axLimit.y = simLimit.y+boundary.distance;
axis([-axLimit.x axLimit.x -axLimit.y axLimit.y])

% specify the bounding box for this circle
boundary.xCenter = [(-simLimit.x):boundary.distance:(simLimit.x) ...
                (-simLimit.x+0.5*boundary.distance):boundary.distance:(simLimit.x-0.5*boundary.distance) ...
                (-simLimit.x):boundary.distance:(simLimit.x) ...
                (-simLimit.x+0.5*boundary.distance):boundary.distance:(simLimit.x-0.5*boundary.distance) ...
                (-simLimit.x):boundary.distance:(simLimit.x)]';
boundary.yCenter = [-simLimit.y -simLimit.y -simLimit.y -simLimit.y -simLimit.y ...
                -sqrt(3)/2*boundary.distance -sqrt(3)/2*boundary.distance -sqrt(3)/2*boundary.distance -sqrt(3)/2*boundary.distance ...
                0 0 0 0 0 ...
                sqrt(3)/2*boundary.distance sqrt(3)/2*boundary.distance sqrt(3)/2*boundary.distance sqrt(3)/2*boundary.distance ...
                simLimit.y simLimit.y simLimit.y simLimit.y simLimit.y]';
```

```
boundary.xMin = -boundary.radius + boundary.xCenter;
boundary.yMin = -boundary.radius + boundary.yCenter;
width = 2*boundary.radius;
height = 2*boundary.radius;


% use the 'curvature' option to draw the circle
for iCell=1:boundary.number
   rectangle('position',[boundary.xMin(iCell) boundary.yMin(iCell) width(iCell) height(iCell)],'curvature',[1 1]);
end

% add a title
title(['diffusion - density:' num2str(boundary.density) ' alpha:' num2str(alpha)] )
drawnow;           % draw the initial distribution
pause(1);          % and pause for a second, so the user can see it

% data set for different diffusion coeffizienz
inout = zeros(particle.nTotal,simTime/deltaT.tred);
for iCell = 1:boundary.number
   xPos = particle.xPos - boundary.xCenter(iCell);
   yPos = particle.yPos - boundary.yCenter(iCell);
   radius = (xPos.^2 + yPos.^2).^.5;
   for iPos = 1:particle.nTotal
      if radius(iPos) < boundary.radius(iCell)
         inout(iPos,:) = 1;
      end
   end
end
out = inout + gainex * ( 1 - inout );

%% initiate main loop

tic;    % start timer for evaluation of execution speed (main loop only)
nSteps = ceil(simTime/deltaT.t);
boundedRadius = zeros(particle.nTotal,1);
if resume == 0
   randomway.x = zeros(particle.nTotal,ceil(simTime/deltaT.tred));
   randomway.y = zeros(particle.nTotal,ceil(simTime/deltaT.tred));
   randomway.z = zeros(particle.nTotal,ceil(simTime/deltaT.tred));
   startStep = 1;
else
   startStep = iStep;
end
iTest = 1;
count = 0;

x=zeros(nSteps,boundary.number);

%% begin main loop

for iStep = startStep:nSteps

   % calculates the way the water molecules would move if there was no
   % restriction. The moved distance is a fix value give by the average
   % way a molecule would move in the given time. The direction is random.
   % This will result in a nearly gausian movement.
   deltaS.r = ones(particle.nTotal,1).*out(:,1).*deltaS.mean;
   deltaS.Phi = rand(particle.nTotal, 1)*2*pi;
   deltaS.Psi = rand(particle.nTotal, 1)*2*pi;
   deltaS.x = ((4/3)^.5)*deltaS.r.*cos(deltaS.Phi).*cos(deltaS.Psi);
   deltaS.y = ((4/3)^.5)*deltaS.r.*sin(deltaS.Phi).*cos(deltaS.Psi);
   deltaS.z = ((2/3)^.5)*deltaS.r.*sin(deltaS.Psi);
   particle.xPos_new = particle.xPos + deltaS.x;
   particle.yPos_new = particle.yPos + deltaS.y;
   particle.zPos_new = particle.zPos + deltaS.z;

   % Particles are reflected at the boundaries of the simulation. These
   % boundaries should be (much) bigger than the regoin of interest to minimize
```

```
    % the systematic error. The boundaries in this simulation are the edges
    % of a square as our ragion of interest is also a square (like the voxel
    % of the MRI signal). It's also faster to compute cause the reflection
    % at a plan surface can be implimented as a matrix calculation. (no
    % loop needed)
    % In order to get a faster calculation, the start position changes each
    % time the particle hits the simulation boundaries. (The distance to
    % the boundary remains the same but it will be on the other side of the
    % boundary. This way it is like outside the boundary the structure is
    % the same as inside. This is possible if the boundaries are chosen
    % whise and the structure is for example hexagonal.)

    % max x value
    reflected = ceil(abs((particle.xPos_new-min(particle.xPos_new,(2*simLimit.x-particle.xPos_new)))./particle.xPos));
    particle.xStart = particle.xStart + 2*reflected.*(simLimit.x-particle.xStart);
    particle.xPos_new = min(particle.xPos_new,(2*simLimit.x-particle.xPos_new));
%     particle.xStart = particle.xStart - 2*boundary.distance*reflected;
%     particle.xPos_new = particle.xPos_new - 2*boundary.distance*reflected;

    % min x value
    reflected = ceil(abs((particle.xPos_new-max(particle.xPos_new,(-2*simLimit.x-particle.xPos_new)))./particle.xPos));
    particle.xStart = particle.xStart + 2*reflected.*(-simLimit.x-particle.xStart);
    particle.xPos_new = max(particle.xPos_new,(-2*simLimit.x-particle.xPos_new));
%     particle.xStart = particle.xStart + 2*boundary.distance*reflected;
%     particle.xPos_new = particle.xPos_new +
%     2*boundary.distance*reflected;

    % max y value
    reflected = ceil(abs((particle.yPos_new-min(particle.yPos_new,(2*simLimit.y-particle.yPos_new)))./particle.yPos));
    particle.yStart = particle.yStart + 2*reflected.*(simLimit.y-particle.yStart);
    particle.yPos_new = min(particle.yPos_new,(2*simLimit.y-particle.yPos_new));
%     particle.yStart = particle.yStart - sqrt(3)*boundary.distance*reflected;
%     particle.yPos_new = particle.yPos_new - sqrt(3)*boundary.distance*reflected;

    % min y value
    reflected = ceil(abs((particle.yPos_new-max(particle.yPos_new,(-2*simLimit.y-particle.yPos_new)))./particle.yPos));
    particle.yStart = particle.yStart + 2*reflected.*(-simLimit.y-particle.yStart);
    particle.yPos_new = max(particle.yPos_new,(-2*simLimit.y-particle.yPos_new));
%     particle.yStart = particle.yStart + sqrt(3)*boundary.distance*reflected;
%     particle.yPos_new = particle.yPos_new + sqrt(3)*boundary.distance*reflected;

    % Calculation of the changed diffusion way due to restricted diffusion
    % caused by cell membranes. To calculate the way, the 0/0 coordinates
    % are placed in the center of the cell of interest.
    for iCell = 1:boundary.number

        % Calculation of the coordinates of the water molecules seen from
        % the center of the cell of interest
        particle.xPos_new = particle.xPos_new - boundary.xCenter(iCell);
        particle.yPos_new = particle.yPos_new - boundary.yCenter(iCell);
        particle.xPos = particle.xPos - boundary.xCenter(iCell);
        particle.yPos = particle.yPos - boundary.yCenter(iCell);

        % compute the radius and angle of the new positions
        radius = (particle.xPos.^2 + particle.yPos.^2).^.5;
        angle = atan2(particle.yPos, particle.xPos);
        radius_new = (particle.xPos_new.^2 + particle.yPos_new.^2).^.5;
        angle_new = atan2(particle.yPos_new, particle.xPos_new);

        % compute values needed in the next loop for faster calculation
        a = (boundary.radius(iCell) - radius)./(radius_new - radius); % part of the random way deltaS.r befor hitting the membrane
        particle.xPos_ref = particle.xPos + a.*(deltaS.x); % x-coordinate of the membrane contact
        particle.yPos_ref = particle.yPos + a.*(deltaS.y); % y-coordinate of the membrane contact
        particle.rPos_ref = (particle.xPos_ref.^2+particle.yPos_ref.^2).^.5;
        a = a.*max(boundary.radius(iCell)./particle.rPos_ref,particle.rPos_ref./boundary.radius(iCell)); % small correction of a systematical
calculation error
        particle.xPos_ref = particle.xPos + a.*(deltaS.x);
        particle.yPos_ref = particle.yPos + a.*(deltaS.y);
```

```
particle.rPos_ref = (particle.xPos_ref.^2+particle.yPos_ref.^2).^.5;
angle_ref = atan2(particle.yPos_ref,particle.xPos_ref);
particle.xway_ref = ( - deltaS.x.*cos(2*angle_ref) - deltaS.y.*sin(2*angle_ref));
particle.yway_ref = ( - deltaS.x.*sin(2*angle_ref) + deltaS.y.*cos(2*angle_ref));
angle_ref12 = 2*(angle_ref - deltaS.Phi) + pi;

% Calculation of the effects caused by restricted diffusion.
for iPos = 1:particle.nTotal
   % Molecules that would pass the boundary dute to brownian motion
   % should be reflected elastic. To calculate this it was necessary
   % to test if the molecule was inside or out side. Molecules that
   % would end exactly at the boundary were set a small part away from
   % the boundary so we can tell in the next iteration step if the
   % molecule was inside or outside.
   % alpha ... chance to penatrated the membrane
   if (rand > alpha)
      if (radius(iPos) < boundary.radius(iCell)) %treatment of molecules inside the boundary
         if (radius_new(iPos) > boundary.radius(iCell))    % treatment of molecules the would have passed the boundary
            i = 0;
            if (abs(sin(angle_ref12(iPos)/2)) < sin(pi/720))
               particle.xPos_new(iPos) = radius(iPos)*cos(angle_ref(iPos) + (1-a(iPos))*deltaS.r(iPos));
               particle.yPos_new(iPos) = radius(iPos)*sin(angle_ref(iPos) + (1-a(iPos))*deltaS.r(iPos));
               i=1001;
            else
               delta1 = 1;
               while (radius_new(iPos) > boundary.radius(iCell) && delta1 > 0)
                  delta = (1-(a(iPos)+i*abs(sin(angle_ref12(iPos)/2)))); % change remaining way length with each reflection
                  phi = angle(iPos)+i*angle_ref12(iPos); % change of the angle of the refleted point on the cell surface
                  beta = angle_ref12(iPos)*i; % change of the direction of the particle with each reflection
                  particle.xPos_new(iPos) = particle.rPos_ref(iPos)*cos(phi) + (particle.xway_ref(iPos)*cos(beta) -
particle.yway_ref(iPos)*sin(beta+pi))*delta;
                  particle.yPos_new(iPos) = particle.rPos_ref(iPos)*sin(phi) + (particle.xway_ref(iPos)*sin(beta) +
particle.yway_ref(iPos)*cos(beta))*delta;
                  radius_new(iPos) = (particle.xPos_new(iPos)^2+particle.yPos_new(iPos)^2).^.5;
                  i = i + 1;
                  if (radius_new(iPos) > boundary.radius(iCell) && delta < abs(sin(angle_ref12(iPos)/2)))
                     delta1 = 0;
                  end
               end
               if (delta1 == 0)
                  particle.xPos_new(iPos) = particle.xPos_new(iPos)*boundary.radius(iCell)*.999/radius_new(iPos);
                  particle.yPos_new(iPos) = particle.yPos_new(iPos)*boundary.radius(iCell)*.999/radius_new(iPos);
               end
            end
         end
         if (radius_new(iPos) == boundary.radius(iCell))    % treatment of molecules that woud end in the boundary
            boundedRadius(iPos) = radius_new(iPos) - .001*boundary.radius(iCell);
            particle.xPos_new(iPos) = boundedRadius(iPos)*cos(angle_new(iPos));
            particle.yPos_new(iPos) = boundedRadius(iPos)*sin(angle_new(iPos));
            count = count + 1;
         end
         x(iStep,iCell) = x(iStep,iCell) + 1;
      else    %treatment of molecules outside the boundary
         if (radius_new(iPos) == boundary.radius(iCell))    % treatment of molecules that woud end in the boundary
            boundedRadius(iPos) = radius_new(iPos) + .001*boundary.radius(iCell);
            particle.xPos_new(iPos) = boundedRadius(iPos)*cos(angle_new(iPos));
            particle.yPos_new(iPos) = boundedRadius(iPos)*sin(angle_new(iPos));
            count = count + 1;
         elseif (radius_new(iPos) < boundary.radius(iCell))    % treatment of molecules the would have passed the boundary
            particle.xPos_new(iPos) = particle.rPos_ref(iPos)*cos(angle_ref(iPos)) + particle.xway_ref(iPos);
            particle.yPos_new(iPos) = particle.rPos_ref(iPos)*sin(angle_ref(iPos)) + particle.yway_ref(iPos);
         end
      end
   end
end

particle.xPos_new = particle.xPos_new + boundary.xCenter(iCell);
particle.yPos_new = particle.yPos_new + boundary.yCenter(iCell);
```

```
      particle.xPos = particle.xPos + boundary.xCenter(iCell);
      particle.yPos = particle.yPos + boundary.yCenter(iCell);

   end

   % Particles are reflected at the boundaries of the simulation. These
   % boundaries should be (much) bigger than the regoin of interest to minimize
   % the systematic error. The boundaries in this simulation are the edges
   % of a square as our ragion of interest is also a square (like the voxel
   % of the MRI signal). It's also faster to compute cause the reflection
   % at a plan surface can be implimented as a matrix calculation. (no
   % loop needed)
   % In order to get a faster calculation, the start position changes each
   % time the particle hits the simulation boundaries. (The distance to
   % the boundary remains the same but it will be on the other side of the
   % boundary. This way it is like outside the boundary the structure is
   % the same as inside. This is possible if the boundaries are chosen
   % whise and the structure is for example hexagonal.)

      % max x value
   reflected = ceil(abs((particle.xPos_new-min(particle.xPos_new,(2*simLimit.x-particle.xPos_new)))./particle.xPos));
   particle.xStart = particle.xStart + 2*reflected.*(simLimit.x-particle.xStart);
   particle.xPos_new = min(particle.xPos_new,(2*simLimit.x-particle.xPos_new));
%    particle.xStart = particle.xStart - 2*boundary.distance*reflected;
%    particle.xPos_new = particle.xPos_new - 2*boundary.distance*reflected;

   % min x value
   reflected = ceil(abs((particle.xPos_new-max(particle.xPos_new,(-2*simLimit.x-particle.xPos_new)))./particle.xPos));
   particle.xStart = particle.xStart + 2*reflected.*(-simLimit.x-particle.xStart);
   particle.xPos_new = max(particle.xPos_new,(-2*simLimit.x-particle.xPos_new));
%    particle.xStart = particle.xStart + 2*boundary.distance*reflected;
%    particle.xPos_new = particle.xPos_new + 2*boundary.distance*reflected;

   % max y value
   reflected = ceil(abs((particle.yPos_new-min(particle.yPos_new,(2*simLimit.y-particle.yPos_new)))./particle.yPos));
   particle.yStart = particle.yStart + 2*reflected.*(simLimit.y-particle.yStart);
   particle.yPos_new = min(particle.yPos_new,(2*simLimit.y-particle.yPos_new));
%    particle.yStart = particle.yStart - sqrt(3)*boundary.distance*reflected;
%    particle.yPos_new = particle.yPos_new - sqrt(3)*boundary.distance*reflected;

   % min y value
   reflected = ceil(abs((particle.yPos_new-max(particle.yPos_new,(-2*simLimit.y-particle.yPos_new)))./particle.yPos));
   particle.yStart = particle.yStart + 2*reflected.*(-simLimit.y-particle.yStart);
   particle.yPos_new = max(particle.yPos_new,(-2*simLimit.y-particle.yPos_new));
%    particle.yStart = particle.yStart + sqrt(3)*boundary.distance*reflected;
%    particle.yPos_new = particle.yPos_new + sqrt(3)*boundary.distance*reflected;

   % calculate the random way each molecule went
   % ceil(iStep/deltaT.tred_fac) ... reduces the time resolution this is
   % needed cause MatLab doesn't allow the size of a to big array
   randomway.x(:,ceil(iStep/deltaT.tred_fac)) = particle.xPos_new - particle.xStart;
   randomway.y(:,ceil(iStep/deltaT.tred_fac)) = particle.yPos_new - particle.yStart;
   randomway.z(:,ceil(iStep/deltaT.tred_fac)) = particle.zPos_new - particle.zStart;

   % re-compute particle positions using the bounded radius
   particle.xPos = particle.xPos_new;
   particle.yPos = particle.yPos_new;
   particle.zPos = particle.zPos_new;

   particle.xResume = particle.xPos;
   particle.yResume = particle.yPos;
   particle.zResume = particle.zPos;

%       % plot the new particle positions
%       set(hplot, 'xdata', particle.xPos,  'ydata', particle.yPos);
%       drawnow;
%       pause(.1)
   if mod (iStep,10) == 0
```

```
      iStep
   end
end
elapsedTime = toc;    % stop timer and save elapsed time
randomway.r = (randomway.x.^2 + randomway.y.^2 + randomway.z.^2).^.5;

% plot the new particle positions
set(hplot, 'xdata', particle.xPos,  'ydata', particle.yPos);
drawnow;
pause(.1)

%% Calculation of the diffusion parameters (ADC and Kurtosis)
% As we use no random way lenght for the calculation of the random way,
% it's necessary to lower the time resolution for the following
% calculations. This way the systematic failure is lower than the nois
% cause by the randomway simulation.
iRed.t = ceil(deltaT.tred/deltaT.t:deltaT.tred/deltaT.t:simTime/deltaT.t);
red.t = iRed.t.*deltaT.t;

% As the radius of the random way has only positve values we need to create
% data with random positive and negative values so we can use the funktions
% std and kurtosis. To achive that, I create random discrete values that
% are either -1 or 1. (2*{1 or 2}-3 is -1 or 1)
%randomway.rkurt = randomway.r.*(2*random('discrete uniform', 2, size(randomway.r)) - 3);

% calculations of the random way length
randomway.xstd = std(randomway.x);
randomway.ystd = std(randomway.y);
randomway.zstd = std(randomway.z);
randomway.rstd = std(randomway.x + randomway.y + randomway.z);
%randomway.rstd = std(randomway.rkurt);
%randomway.rstdFast = std(randomway.r.*(1-inout)).*(length(randomway.r)/(length(randomway.r)-sum(inout(:,1))));
%randomway.rstdSlow = std(randomway.r.*inout).*(length(randomway.r)/sum(inout(:,1)));

% calculation of ADC and kurtosis
% calculation of kurtosis of r:
% using r = x+y+z instead of r' = sqrt(x^2+y^2+z^2)
% cause number of value with |r'| < e for e element of R and e>0
% would be to low and therefore the calculation of the kurtosis
% would be wronge! (kurtosis would be -1.5 cause of that.)
% But as: var(x + y) = var(x) + var(y) = var(sqrt(x^2 + y^2)
% and: kurtosis = mean(r^4)/var(r)
% kurtosis = mean((x+y+z)^4)/var(x+y+z)
ADC.x = (randomway.xstd.^2)./((red.t).*6);
ADC.xkurt = kurtosis(randomway.x)-3;
ADC.y = (randomway.ystd.^2)./((red.t).*6);
ADC.ykurt = kurtosis(randomway.y)-3;
ADC.z = (randomway.zstd.^2)./((red.t).*6);
ADC.zkurt = kurtosis(randomway.z)-3;
ADC.r = (randomway.rstd.^2)./((red.t).*6);
ADC.rkurt = kurtosis(randomway.x + randomway.y + randomway.z)-3;
%ADC.rFast = (randomway.rstdFast.^2)./((red.t).*4);
%ADC.rSlow = (randomway.rstdSlow.^2)./((red.t).*4);

% print out some diagnostics
fprintf('Simulating %d particles for %d steps required %.2f seconds.\n',...
   particle.nTotal, nSteps, elapsedTime);

% Estemating the kurtosis and ADC for intra and extracellular matter.

in = 1;
out = 1;
randomway.xin = zeros(sum(inout(:,1)),ceil(simTime/deltaT.tred));
randomway.yin = zeros(sum(inout(:,1)),ceil(simTime/deltaT.tred));
randomway.zin = zeros(sum(inout(:,1)),ceil(simTime/deltaT.tred));
randomway.xout = zeros(particle.nTotal - sum(inout(:,1)),ceil(simTime/deltaT.tred));
randomway.yout = zeros(particle.nTotal - sum(inout(:,1)),ceil(simTime/deltaT.tred));
randomway.zout = zeros(particle.nTotal - sum(inout(:,1)),ceil(simTime/deltaT.tred));
```

```
for l = 1:particle.nTotal
   if inout(l,1) == 1;
     randomway.xin(in,:) = randomway.x(l,:);
     randomway.yin(in,:) = randomway.y(l,:);
     randomway.zin(in,:) = randomway.z(l,:);
     in = in + 1;
   else
     randomway.xout(out,:) = randomway.x(l,:);
     randomway.yout(out,:) = randomway.y(l,:);
     randomway.zout(out,:) = randomway.z(l,:);
     out = out + 1;
   end
   if mod(l,100) == 0
      l
   end
end

randomway.xinstd = std(randomway.xin);
randomway.yinstd = std(randomway.yin);
randomway.zinstd = std(randomway.zin);
randomway.rinstd = std(randomway.xin + randomway.yin + randomway.zin);

randomway.xoutstd = std(randomway.xout);
randomway.youtstd = std(randomway.yout);
randomway.zoutstd = std(randomway.zout);
randomway.routstd = std(randomway.xout + randomway.yout + randomway.zout);

ADC.xin = (randomway.xinstd.^2)./((red.t).*6);
ADC.xinkurt = kurtosis(randomway.xin)-3;
ADC.yin = (randomway.yinstd.^2)./((red.t).*6);
ADC.yinkurt = kurtosis(randomway.yin)-3;
ADC.zin = (randomway.zinstd.^2)./((red.t).*6);
ADC.zinkurt = kurtosis(randomway.zin)-3;
ADC.rin = (randomway.rinstd.^2)./((red.t).*6);
ADC.rinkurt = kurtosis(randomway.xin + randomway.yin + randomway.zin)-3;

ADC.xout = (randomway.xoutstd.^2)./((red.t).*6);
ADC.xoutkurt = kurtosis(randomway.xout)-3;
ADC.yout = (randomway.youtstd.^2)./((red.t).*6);
ADC.youtkurt = kurtosis(randomway.yout)-3;
ADC.zout = (randomway.zoutstd.^2)./((red.t).*6);
ADC.zoutkurt = kurtosis(randomway.zout)-3;
ADC.rout = (randomway.routstd.^2)./((red.t).*6);
ADC.routkurt = kurtosis(randomway.xout + randomway.yout + randomway.zout)-3;

% % Minimize the noise of the kurtosis as the the noise of the results of
% % the Simulations effect the calculated Kurtosis with the 4th order
%
% ADC.rkurtm = zeros(size(ADC.rkurt));
% ADC.rm = zeros(size(ADC.r));
% ADC.rinkurtm = zeros(size(ADC.rinkurt));
% ADC.rinm = zeros(size(ADC.rin));
% ADC.routkurtm = zeros(size(ADC.routkurt));
% ADC.routm = zeros(size(ADC.rout));
% for i=1:length(ADC.rkurt)
%    if i<10
%       ADC.rkurtm(i) = mean(ADC.rkurt(1:i+9))*(i+9)/19;
%       ADC.rm(i) = mean(ADC.r(1:i+9));
%       ADC.rinkurtm(i) = mean(ADC.rinkurt(1:i+9))*(i+9)/19;
%       ADC.rinm(i) = mean(ADC.rin(1:i+9));
%       ADC.routkurtm(i) = mean(ADC.routkurt(1:i+9))*(i+9)/19;
%       ADC.routm(i) = mean(ADC.rout(1:i+9));
%    elseif i<length(ADC.rkurt)-9
%       ADC.rkurtm(i) = mean(ADC.rkurt(i-9:i+9));
%       ADC.rm(i) = mean(ADC.r(i-9:i+9));
%       ADC.rinkurtm(i) = mean(ADC.rinkurt(i-9:i+9));
%       ADC.rinm(i) = mean(ADC.rin(i-9:i+9));
```

```
%        ADC.routkurtm(i) = mean(ADC.routkurt(i-9:i+9));
%        ADC.routm(i) = mean(ADC.rout(i-9:i+9));
%     else
%        ADC.rkurtm(i) = mean(ADC.rkurt(i-9:length(ADC.rkurt)));
%        ADC.rm(i) = mean(ADC.r(i-9:length(ADC.r)));
%        ADC.rinkurtm(i) = mean(ADC.rinkurt(i-9:length(ADC.rkurt)));
%        ADC.rinm(i) = mean(ADC.rin(i-9:length(ADC.r)));
%        ADC.routkurtm(i) = mean(ADC.routkurt(i-9:length(ADC.rkurt)));
%        ADC.routm(i) = mean(ADC.rout(i-9:length(ADC.r)));
%     end
% end

%% diff/kurt berechnung (fit)

S = zeros(50,length(red.t));
for t = 1:length(red.t)
   for b = 1:1:50
      S(b,t) = 1/size(randomway.x,1)*sum(cos((randomway.x(:,t) + randomway.y(:,t) + randomway.z(:,t))*sqrt(b/(3*t))));
   end
end

fckurt = 'exp(-b(1)*x + 1/6*b(1)^2*b(2)*x.^2)';
fcbi = '(1-a(1))*exp(-a(2)*x) + a(1)*exp(-a(3)*x)';
fakurt = inline(fckurt,'b','x');
fabi = inline(fcbi,'a','x');
xd = .1:.1:5;
as2 = [1,.7];
as1 = [0.7,1.5,0.7];

for b=10:1:50
   for t = red.t(10:length(red.t))
      ADCfit(b,:) = nlinfit(xd(1:b),S(1:b,t)',fakurt,as2);
      ADC2fit(b,:) = nlinfit(xd(1:b),(S(1:b,t)' + 22/508)/(1+22/508),fakurt,as2);
      biexfit(b,t:) = nlinfit(xd(1:b),S(1:b,t)',fabi,as1);
      biex2fit(b,:) = nlinfit(xd(1:b),max(S(1:b,t),14/177)',fabi,as1);
      ADC.dfit(b,t) = ADCfit(b,1);
      ADC.kfit(b,t) = ADCfit(b,2);
      ADC.dfit2(b,t) = ADC2fit(b,1);
      ADC.kfit2(b,t) = ADC2fit(b,2);
      ADC.abiex(b,t) = biexfit(b,1);
      ADC.bbiex(b,t) = biexfit(b,2);
      ADC.cbiex(b,t) = biexfit(b,3);
      ADC.abiex2(b,t) = biex2fit(b,1);
      ADC.bbiex2(b,t) = biex2fit(b,2);
      ADC.cbiex2(b,t) = biex2fit(b,3);
   end
end
```

Bibliography

[1] A.A. Markov. "Extension of the limit theorems of probability theory to a sum of variables connected in a chain". reprinted in Appendix B of: R.Howard. Dynamic Probabilistic Systems, volume 1: Markov Chains. John Wiley and Sons, 1971.

[2] A. Papoulis. Probability, Random Variables and Stochastic Processes. McGraw-Hill, Tokyo, Japan, 2nd edition, 1984.

[3] Amiry-Moghaddam M and Ottersen O P 2003: The Molecular Basis of Water Transport in the Brain. Nat. Rev. Neurosci. 4 991–1001.

[4] Assaf Y and Cohen Y 1998: Non-mono-exponential Attenuation of Water and N-acetyl Aspartate Signals due to Diffusion in Brain Tissue. J. Magn. Reson. 131 69–85.

[5] Bloch F, Nuclear Induction, Physical Review 70, 460-473 (1946)

[6] Denis Le Bihan: Molecular Diffusion Nuclear Magnetic Resonance Imaging, M.R. Quarterly 7(1), pp. 1-30, 1991.

[7] Denis Le Bihan, R. Turner and P. Douek 1993: Is Water Diffusion Restricted in Human Brain White Matter? An Echo-planar NMR Imaging Study. Neuro. Rep. 4 887–90.

[8] Denis Le Bihan 2003: Looking into the Functional Architecture of the Brain with Diffusion MRI. Nat. Rev. Neurosci. 4 469–80.

[9] Denis Le Bihan: The 'Wet Mind': Water and Functional Neuroimaging Phys. Med. Biol. 52 (2007) R57-R90.

[10] Richard B. Buxton: Introduction to Functional Magnetic Resonance Imaging: Principles and Techniques. Cambridge University Press, 2002.

[11] Chang D C, Rorschach H E, Nichols B L and Hazlewood C F 1973: Implications of Diffusion Coefficient Measurements for the Structure of Cellular Water. Ann. NY Acad. Sci. 204 434–43.

[12] Chen K C and Nicholson C 2000: Changes in Brain Cell Shape Create Residual Extracellular Space Volume and Explain Tortuosity Behavior During Osmotic Challenge. Proc. Natl Acad. Sci. USA 97 8306–11.

[13] Chin, C.L., Wehrli, F.W., Fan, Y., Hwang, S.N., Schwartz, E.D., Nissanov, J., Hackney, D.B., 2004: Assessment of Axonal Fiber Tract Architecture in Excised Rat Spinal Cord by Localized NMR q-space Imaging: Simulations and Experimental Studies. Magn. Reson. Med. 52, 733–740.

[14] Cohen Y and Assaf Y 2002: High b-value q-space Analyzed Diffusion-weighted MRS and MRI in Neuronal Tissues—a Technical Review NMR. Biomed. 15 516–42.

[15] Colsenet R, Mariette F and Cambert M 2005: NMR Relaxation and Water Self-diffusion Studies in whey Protein Solutions and gels. J. Agric. Food. Chem. 53 6784–90.

[16] Einstein A., Annalen der Physik, 1905, S. 549 ff.

[17] Els Fieremans, Yves De Deene, and Ignace Lemahieu: VALIDATION OF MODELS FOR THE DIFFUSION WEIGHTED MR SIGNAL IN BRAIN WHITE MATTER. ©2008 IEEE-978-1-4244-2003-2/08. 915-918.

[18] Daniel Güllmar, Jens Haueisen, and Jürgen R. Reichenbach: Analysis of b-value Calculation in Diffusion Weighted and Diffusion Tensor Imaging. Concepts of Magnetic Resonance Part A, 25A(1):53-66, 2005.

[19] Harris KR, Woolf LA: Pressure and Temperature Dependence of the Self Diffusion Coefficient of Water and Oxygen-18 water. J Chem Soc– Faraday Trans I 1980;76:377–385.

[20] Hazlewood C F, Rorschach H E and Lin C 1991: Diffusion of Water in Tissues and MRI. Magn. Reson. Med. 19 214–6.

[21] Jan C. J. Bart: Plastics Additives: Advanced Industrial Analysis. ISBN-10: 1586035339, ISBN-13: 978-1586035334, January 1, 2006

[22] King, M.D., Houseman, J., Gadian, D.G., Connelly, A., 1997: Localized q-space Imaging of the Mouse Brain. Magn. Reson. Med. 38, 930–937.

[23] Kroenke CD, Ackerman JJ, and Yablonskiy DA: On the Nature of the NAA Diffusion Attenuated MR Signal in the Central Nervous System. Magn Reson Med. 2004; 52(5):1052–1059. [PubMed: 15508157]

[24] Leonid I. Rudin1, Stanley Osherand Emad Fatemi, North-Holland Nonlinear total variation based noise removal algorithms* Cognitech Inc., 2800, 28th Street, Suite 101, Santa Monica, CA 90405, USA, D Physica 60 (1992) 259-268

[25] M. Mächler: Very Smooth Nonparametric Curve Estimation by Penalizing Change of Curvature. Technical Report 71, ETH Zurich, May 1993 [6].

[26] Ludovico Minati, Domenico Aquino, Stefano Rampoldi, Sergio Papa, Marina Grisoli, Maria Grazia Bruzzone, Elio Maccagnano: Biexponential and Diffusional Kurtosis Imaging, and Generalised Diffusion-Tensor Imaging (GDTI) with rank-4 Tensors: a Study in a Group of Healthy Subjects. Magn Reson Mater Phy (2007) 20:241–253.

[27] Mitra, P., Halperin, B., 1995: Effect of Finite Gradient Pulse Width in Pulsed Gradient Diffusion Measurements. J. Magn. Reson., Ser. A 113, 94–101.

[28] Moonen C T W, Pekar J, De Vleeschouwer M H M, Van Gelderen P, Van Zijl P C M and Des Pres D 1991: Restricted and Anisotropic Displacement of Water in Healthy cat Brain and in Stroke Studied by NMR Diffusion Imaging. Magn. Reson. Med. 19 327–32.

[29] Moseley ME, Cohen Y, Mintorovitch J, Chileuitt L, Shimizu H, Kucharczyk J, Wendland MF, and Weinstein PR: Early Detection of Regional Cerebral Ischemia in Cats: Comparison of Diffusion- and T2-weighted MRI and Spectroscopy. *Magnetic Resonance in Medicine.* 1990;14(2):330–346. [PubMed].

[30] http://www.nhsdirect.wales.nhs.uk/encyclopaedia/c/article/cerebrovasculardisease: Cerebrovascular disease.

[31] Nicholson C and Philipps J M 1981: Ion Diffusion Modified by Tortuosity and Volume Fraction in the Extracellular Micorenvrionment of the Rat Cerebellum J. Physiol. 321 225–57.

[32] Charles Nicholson and Eva Sykova: Extracellular Space Structure Revealed by Diffusion Analysis. Trends Neurosci. (1998) 21, 207–215.

[33] Niendorf T, Dijkhuizen R M, Norris D G, Van Lookeren Campagne M and Nicolay K 1996: Biexponential Diffusion Attenuation in Various States of Brain Tissue: Implications for Diffusion-weighted Imaging. Magn. Reson. Med. 36 847–57.

[34] Henry H. Ong, Alex C. Wright, Suzanne L. Wehrli, Andre Souza, Eric D. Schwartz, Scott N. Hwang, and Felix W. Wehrli: Indirect Measurement of Regional Axon Diameter in Excised Mouse Spinal Cord with q-space Imaging: Simulation and Experimental Studies. www.elsevier.com/locate/ynimg NeuroImage 40 (2008) 1619–1632.

[35] Patasius, M., Marozas, V., Lukosevicius, A., and Jegelevicius, D.: Evaluation of Tortuosity of eye Blood Vessels Using the Integral of Square of Derivative of Curvature. EMBEC'05: Proceedings of the 3rd IFMBE European Medical and Biological Engineering Conference, November 20 - 25, 2005, Prague. - ISSN 1727-1983. - Prague. - 2005, Vol. 11, p. [1-4].

[36] Rorschach H E, Chang D C, Hazlewood C F and Nichols B L 1973: The Diffusion of Water in Striated Muscle. Ann. NY Acad. Sci. 204 445–52.

[37] Rothwell, PM: "Effect of Urgent Treatment of Transient Ischemic Attack and Minor Stroke on Early Recurrent Stroke (EXPRESS study): a Prospective Population-based Sequential Comparison." Neurology. 2007 DOI:10.1016/S0140-6736(07)61448-2.

[38] Sehy JV, Ackerman JJ, and Neil JJ: Apparent Diffusion of Water, Ions, and Small Molecules in the Xenopus oocyte is Consistent with Brownian Displacement. Magn Reson Med. 2002; 48(1):42–51. [PubMed: 12111930].

[39] Shah SH, Saver JL, Kidwell CS, Albers GW, Rothwell PM, Ay H, Koroshetz WJ, Inatomi Y, Uchino M, Demchuk AM, Coutts SB, Purroy F, Alvarez-Sabin JS, Sander D, Sander K, Restrepo L, Wityk RJ, Marx JJ, and Easton JD: A Multicenter Pooled, Patient-level Data Analysis of Diffusion-weighted MRI in TIA Patients. Stroke. 2007;38:463..

[40] Stanisz G J, Szafer A, Wright G A and Henkelman R M 1997: An Analytical Model of Restricted Diffusion in Bovine Optic Nerve. Magn. Reson. Med. 37 103–11.

[41] Stejskal E.O., and Tanner J.E.: Spin Diffusion Measurements: Spin Echoes in the Presence of a Time Dependent Field Gradient, Journal of Chemical Physics 42(1), pp. 226-292, 1965.

[42] Stroke.org.: Transient Ischemic Attack (TIA): Prognosis and Key Management Considerations. ABCD2 Score.

[43] Torrey, H. C. (1956). "Bloch Equations with Diffusion Terms". Physical Review 104 (3): 563.

[44] Kazuko Tanaka J.: Chem. Soc., Faraday Trans. 1, 1978, 74, 1879-1881.

[45] Walker HK, Hall WD, and Hurst JW: Clinical Methods: The History, Physical, and Laboratory Examinations. 3rd edition. Boston: Butterworths; 1990.

[46] Warach S, Chien D, Li W, Ronthal M, and Edelman RR: Fast Magnetic Resonance Diffusion-weighted Imaging of Acute Human Stroke. *Neurology*. 1992;42(9):1717.

[47] World Health Organisation (1978): Cerebrovascular Disorders (Offset Publications). Geneva: World Health Organization. ISBN 9241700432. OCLC 4757533.

[48] World Health Organisation (2004): The global burden of disease: 2004 update. ISBN 978 92 4 156371 0.

[49] World Health Organisation (2009): Global Health Risks: Mortality and Burden of Disease Attributable to Selected Major Risks. ISBN 978 92 4 156387 1.